Elastic models of magma reservoir mechanics: a key tool for investigating planetary volcanism

ERIC B. GROSFILS[1]*, PATRICK J. MCGOVERN[2], PATRICIA M. GREGG[3], GERALD A. GALGANA[2,4], DEBRA M. HURWITZ[1,2], SYLVAN M. LONG[1,5] & SHELLEY R. CHESTLER[1,6]

[1]*Geology Department, Pomona College, Claremont, CA 91711, USA*

[2]*Lunar and Planetary Institute, USRA, Houston, TX 77058, USA*

[3]*College of Earth, Ocean, and Atmospheric Science, Oregon State University, Corvallis, OR 97331, USA*

[4]*AIR Worldwide, 131 Dartmouth Street, Boston, MA 02116, USA*

[5]*Leggette, Brashears & Graham Inc., 4 Research Drive, Shelton, CT 06484, USA*

[6]*Department of Earth and Space Sciences, University of Washington, Seattle, WA 98195, USA*

**Corresponding author (e-mail: egrosfils@pomona.edu)*

Abstract: Understanding how shallow reservoirs store and redirect magma is critical for deciphering the relationship between surface and subsurface volcanic activity on the terrestrial planets. Complementing field, laboratory and remote sensing analyses, elastic models provide key insights into the mechanics of magma reservoir inflation and rupture, and hence into commonly observed volcanic phenomena including edifice growth, circumferential intrusion, radial dyke swarm emplacement and caldera formation. Based on finite element model results, the interplay between volcanic elements – such as magma reservoir geometry, host rock environment (with an emphasis on understanding how host rock pore pressure assumptions affect model predictions), mechanical layering, and edifice loading with and without flexure – dictates the overpressure required for rupture, the location and orientation of initial fracturing and intrusion, and the associated surface uplift. Model results are either insensitive to, or can readily incorporate, material and parameter variations characterizing different planetary environments, and they also compare favourably with predictions derived from rheologically complex, time-dependent formulations for a surprisingly diverse array of volcanic scenarios. These characteristics indicate that elastic models are a powerful and useful tool for exploring many fundamental questions in planetary volcanology.

After decades of planetary exploration it is clear that silicic volcanism has been, and remains, one of the primary geological processes controlling the surface evolution of large rocky bodies in our solar system. From myriad studies and observations of igneous processes on Earth and other bodies, it is known that eruption dynamics are closely linked to the complex physical and chemical evolution magma undergoes during ascent, as well as the environmental conditions it encounters at or near the surface (for recent summaries see Sigurdsson *et al.* 2000; Zimbelman & Gregg 2000; Cashman & Sparks 2013). These factors, in turn, help dictate the morphology of the resulting volcanic landforms.

Magma can move rapidly and directly from where it forms to the surface, but the process of ascent commonly occurs in stages, with molten material pausing at one or more depths along the way. In general, stalled magma will either freeze in place to become part of the lithosphere or, if the flux is sufficient, magma accumulation can form reservoirs (cf. Schöpa & Annen 2013 and references therein). Building on decades of previous analyses (e.g. Sparks *et al.* 1977; Hildreth 1981; Christensen & DePaolo 1993; Bachmann & Bergantz 2004; de Silva *et al.* 2006), a considerable array of field, petrological, geochemical and geophysical evidence gathered in recent years indicates that large bodies of magma form periodically and can become eruptible quite rapidly at shallow depth, often within a few kilometres of the surface (e.g. Burgisser & Bergantz 2011; Druitt *et al.* 2012; Gertisser *et al.* 2012; Gualda *et al.* 2012; Huber *et al.* 2012; Matthews *et al.* 2012). Understanding the mechanics underpinning how shallow reservoirs store and redirect near-surface magma is thus critical for deciphering the links between surface and subsurface volcanic activity.

From: Platz, T., Massironi, M., Byrne, P. K. & Hiesinger, H. (eds) *Volcanism and Tectonism Across the Inner Solar System*. Geological Society, London, Special Publications, **401**, http://dx.doi.org/10.1144/SP401.2

In this contribution, we summarize key results from several recent dry rock numerical modelling studies that re-examine how reservoirs redirect magma through inflation and rupture. Motivated, in part, by the apparent rapidity with which eruptible reservoirs can form, the emphasis here is upon models employing an elastic rheology. Elastic models are easily implemented and, although simple, are none the less capable of providing powerful insight into commonly observed reservoir-derived volcanic features such as central eruptions that feed edifice growth, circumferential intrusions, subsurface systems of radial dykes and equant calderas. These volcanic features exhibit remarkably consistent overarching physical and morphological characteristics irrespective of scale or where in the solar system they are found. Although elastic methods have been used to study the mechanics of internally pressurized magma reservoirs for some time (e.g. Anderson 1936; Mogi 1958; Dieterich & Decker 1975; Muller & Pollard 1977; Blake 1981; Davis 1986; McTigue 1987; Yang *et al.* 1988; Tait *et al.* 1989; Sartoris *et al.* 1990; Zuber & Mouginis-Mark 1992; Parfitt *et al.* 1993; Chadwick & Dieterich 1995; Koenig & Pollard 1998; Bonaccorso & Davis 1999; Fialko *et al.* 2001; Pinel & Jaupart 2003; Trasatti *et al.* 2005; Gudmundsson 2012), systematic re-examination is needed because many previous models adopt an 'overpressure only' formulation that implies specific reservoir-proximal pore pressure conditions that are difficult to create and sustain. Using more conservative dry rock elastic models to investigate common volcanic scenarios establishes a baseline framework critical for advancing our understanding of planetary volcanism and, by creating benchmarks against which more sophisticated models can be calibrated, this framework contributes robustly to the groundwork upon which future quantitative explorations of planetary volcanism can build.

Methods

Finite element models implemented within COMSOL Multiphysics (www.comsol.com), which solves Navier–Cauchy equations for linear elastic stress and displacement in response to applied loads, have been used by the authors to simulate a magma reservoir as an internally pressurized cavity within an axisymmetrical, gravitationally loaded host rock of sufficient lateral and vertical extent that edge effects become negligible (Fig. 1). A general summary of this approach is provided below; full model details, including descriptions of physical parameter ranges explored, can be found in the papers cited.

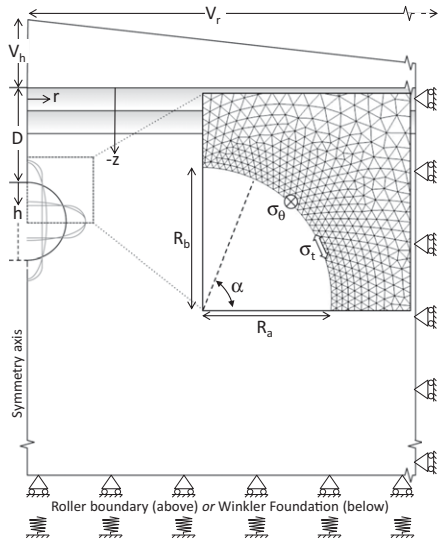

Fig. 1. Illustration of axisymmetrical finite element model geometry using a spherical reservoir example. Inset shows a sample of the mesh near the reservoir wall (at lower resolution than actual, for clarity), the rupture location at angle α, and the two wall-parallel principal stresses σ_θ (out of the plane of the page) and σ_t (within the plane of the page). Part of a conical edifice of axial height V_h and full radius V_r is depicted, as are two mechanical layers (shaded); the edifice and layers are present only in some simulations. The outer and basal edges of the model are subjected to a roller constraint; however, in flexural models, a Winkler foundation is applied to the base instead.

By convention, compressive stresses in the models are negative, and depth z is negative downwards. Mesh elements vary in size, with tens of metres of resolution or less typical near areas of interest (e.g. near the reservoir wall) transitioning into coarser elements in more distal areas. In response to the interplay between the host rock stresses and those applied to the interior of the reservoir wall, COMSOL calculates stresses (σ_r, σ_z, σ_θ, σ_{rz}) throughout the volume in polar cylindrical coordinates, from which the remaining principal stresses normal and tangential to the reservoir wall are derived (Grosfils 2007). Comparing individual applied load components, described below, to standard analytical benchmarks reveals that existing numerical model solutions exhibit maximum percentage errors $\ll 1\%$, which typically translates to absolute displacement differences of the order of 10^{-4}–10^{-5} m and absolute stress differences of the order of 10^{-3} MPa at the reservoir wall (e.g. Grosfils 2007); similar results are reported from calibration tests performed independently (Hobbs 2011).

Host rock boundary conditions and stress state

Gravitational loading in the host rock ($z \leq 0$ m) is implemented via body forces ($\rho_r g$; g is negative) and the application of a lithostatic ($\sigma_z = \sigma_r = \sigma_\theta = -\rho_r g z$) prestress; while alternative stress state end-members exist (e.g. McGarr 1988) and have been assessed to some extent (e.g. Sartoris *et al.* 1990; McGovern & Solomon 1993; Grosfils 2007), their viability in volcanic terrain remains unclear (Grosfils 2007; Gudmundsson 2012), and discussion is restricted here to lithostatic conditions. The host rock is assumed to be dry; that is, pore pressure is negligible. The left-hand boundary ($r = 0$ m), corresponding to the rotation axis, is free to displace vertically. Similarly, implementation of roller boundary conditions along the outer and lower edges of the model ensures that only vertical and lateral displacements, respectively, occur along these margins. The upper boundary of the model space ($z = 0$ m), representing the horizontal surface of the lithosphere, is free to displace.

An exception to the basic model configuration described above occurs when a conical volcanic edifice (or other topography) is introduced. Instead of applying a downwards-directed stress at the $z = 0$ m surface to simulate the weight of a volcano (e.g. Pinel & Jaupart 2003), each edifice is constructed explicitly to ensure that coupling between the load and response is fully integrated into the model. Body forces continue to be applied throughout the edifice, but the optimal prestress state depends on the application being simulated. End-members range from no prestress (in essence, modelling very rapid construction of the edifice relative to the timescales needed for stress equilibration) to a configuration in which the applied lithostatic prestress incorporates the edifice load as part of the vertical column and, hence, varies as a function of distance from the rotation axis. Within the broader model space, the upper surface, whether defined by the flanks of the edifice or the flat regions surrounding it, remains free of displacement constraints, and boundary conditions at the vertical edges of the model are not altered. The lithosphere can continue to be treated as rigid through sustained use of a roller boundary condition along the lower edge of the domain (e.g. Hurwitz *et al.* 2009). Alternatively, a flexural response can be introduced, in which case the roller boundary condition along the base is replaced by a combination of two terms: a 'Winkler' buoyant restoring stress (Watts 2001) that acts to resist deflection of the lithosphere into the underlying fluid asthenosphere; and a stress required for equilibrium that is equal and opposite to the vertical component of the edifice-free lithostatic load at the base of the model (Galgana *et al.* 2011). These terms can also be augmented with additional basal loading as desired, for instance to simulate plume impingement or underplating processes (Galgana *et al.* 2013).

Reservoir boundary conditions

To simulate magma pressure, a normal stress P_m is applied to the interior of the reservoir wall; because the intent is to simulate the magma as a simple, potentially eruptible fluid, no shear stress tractions are imposed. This normal stress is defined as:

$$P_m = [\rho_r g D + \Delta P] + \rho_m g h \quad (1)$$

where ρ_r and ρ_m are the host rock and magma densities, g is gravitational acceleration (negative), ΔP is the overpressure (negative) and the remaining terms are defined in Figure 1. The terms in brackets are applied uniformly at all depths, h, within the reservoir, while the final term varies with h and is thus depth dependent. At the crest of the reservoir ($z = D$), where $h = 0$ m, the first term counters the lithostatic load of the rock column; in essence, creating a state of equilibrium with the surrounding host rock (i.e. in the absence of other contributing stress factors the magma chamber is mechanically stable), while the second term introduces an excess uniform pressure, defined here as the overpressure, that disturbs this equilibrium and, hence, will drive reservoir inflation (or deflation). In models that incorporate a volcano at the surface, an additional, edifice geometry-dependent term is included to offset the additional load (Hurwitz *et al.* 2009; Galgana *et al.* 2011).

Reservoir failure criteria

In response to inflation, simulated by gradually increasing the magnitude of the overpressure ΔP and thereby P_m, outwards displacement can lead to surface deformation, as well as shear and/or tensile rupture of the reservoir wall; shear failure typically requires less overpressure (Gerbault 2012). Mohr–Coulomb criteria can be used to evaluate when and where initial shear failure will take place. Given an angle of internal friction, ϕ, and cohesion, C, shear failure occurs on a fault plane when:

$$\tau \geq -\sigma_n \tan\phi + C \quad (2)$$

where τ is the shear stress and σ_n is the normal stress (negative). Within the host rock, the expected Mohr–Coulomb fault planes develop at angles of

$$\pm\left(45 - \frac{\phi}{2}\right) \quad (3)$$

relative to the maximum compressive stress direction. If sufficient magma intrudes along a fault at the site of shear failure at the reservoir wall, a possibility proposed to explain observations at some locations (e.g. Gerbault 2012; Xu *et al.* 2013), this could alleviate the overpressure. However, observations of seismicity at actively inflating volcanic systems suggest that shear failure proximal to the reservoir, although common, most often does not lead to significant intrusion (e.g. Moran *et al.* 2011; Parks *et al.* 2012). If the overpressure continues to increase, tensile failure will occur once the depth-dependent, expansion-induced, wall-parallel tension within the host rock at the magma–rock interface equals the sum of the factors resisting failure at a given depth (i.e. the wall-parallel component of the lithostatic stress augmented by the tensile strength, T, of the material). Tensile failure is, in some senses, a practical limiting factor when exploring inflation conditions within a reservoir, since release of magma from the reservoir via an intrusion will relieve the overpressure driving outwards displacement (cf. Geyer & Bindeman 2011).

Dry rock model v. 'overpressure only' formulation

Most analytical and numerical simulations of magma reservoir inflation and failure reduce the model system to a cavity inflated solely by overpressure (i.e. $g = 0\ \mathrm{m\ s^{-2}}$ in equation 1) within an unloaded ($\sigma_z = \sigma_r = \sigma_\theta = 0$ MPa) host material. A recent review of magma reservoir mechanics summarizes this 'overpressure only' formulation and, drawing on hydraulic fracturing mathematics and data, offers a three-point critique of the dry rock numerical model approach (Gudmundsson 2012). Before proceeding to a summary of several key results, and discussion of broader implications for understanding reservoir-derived planetary volcanism, it is useful to explore in detail the differences between a dry rock approach and traditional 'overpressure only' model assumptions, and to assess the criticisms levied. In short, different assumptions about host rock conditions are embedded within each modelling approach – this is a critical factor that should be considered carefully before adopting or interpreting the results from either one formulation or the other.

Hydraulic fracture, dry rock. To first order the standard equation for hydraulic failure of a borehole under lithostatic conditions, neglecting thermal stresses and adjusting for the sign convention described above, is given by Zoback (2010, p. 220) as:

$$T = 2\sigma - 2P_\mathrm{p} - (P_\mathrm{m} - P_\mathrm{p}) \tag{4}$$

where P_p is the pore pressure (negative) in the host rock, T is the tensile strength (positive) and σ denotes the least compressive stress magnitude (negative) in the host rock. In the current inflation application, since lithostatic conditions are applied and far-field tectonic stresses are neglected, at the rock–fluid interface σ can be considered the lithostatic stress magnitude parallel to the borehole/reservoir wall. If one assumes negligible pore pressure in the host rock ($P_\mathrm{p} = 0$ MPa), hydraulic failure becomes possible once (cf. section 8.10 of Jaeger & Cook 1979):

$$P_\mathrm{m} = 2\sigma - T. \tag{5}$$

This is the standard failure criterion theory for borehole rupture in dry, unfractured rock, and it indicates that fluid pressure P_m within the borehole must reach approximately twice the lithostatic stress value in the surrounding host rock before rupture of the wall will occur. Complementing this theory, there is both field and laboratory evidence that such overpressures are, indeed, required to rupture rock when negligible pore pressure exists (e.g. Lockner & Byerlee 1977; Jaeger & Cook 1979, p. 226). Recalling that the overpressure is defined here as the uniform pressure in excess of lithostatic (equation 1), another way of presenting this criterion is to state that, for a borehole to rupture:

$$\Delta P = \sigma - T. \tag{6}$$

This is simply the elastic limit for an internally pressurized cylinder in the absence of other normal loads (p. 60 of Timoshenko & Goodier 1951), that is a dry rock borehole formulation. Proceeding in the same vein, if one examines instead an internally pressurized sphere far from the free surface, then the analogous analytically derived criterion for failure becomes (Timoshenko & Goodier 1951, p. 359; Grosfils 2007):

$$\Delta P = 2(\sigma - T). \tag{7}$$

The conditions necessary for rupture can be corrected for the presence of the free surface (e.g. McTigue 1987; Gudmundsson 1988; Parfitt *et al.* 1993; Grosfils 2007), but, in essence, the geometric difference between the borehole and the reservoir affects how stress concentrates during inflation: roughly twice as much pressure is required to rupture an inflating sphere.

Hydraulic fracture, elevated pore pressure. As an alternative condition in the host rock, if one assumes very high pore pressure (lithostatic, i.e. $P_\mathrm{p} = \sigma$) then, returning to equation (4), it quickly becomes apparent that hydraulic fracture of a borehole will occur once:

$$P_\mathrm{m} = \sigma - T, \tag{8}$$

that is, when

$$\Delta P = -T. \tag{9}$$

Similarly, if one reassesses the analytical criterion for failure of a spherical reservoir in the presence of lithostatic pore pressure (replacing σ_t with $\sigma - P_p$ in equation 35 of Grosfils 2007), then

$$\Delta P = 2(\sigma - T - P_p) = -2T. \tag{10}$$

Comparing the high pore pressure results for the borehole and spherical reservoir, it is once again apparent that twice as much overpressure is required to rupture the reservoir. In addition, however, comparison between the equations for failure under dry rock conditions with those that assume lithostatic pore pressure reveals that dry rock conditions require significantly higher fluid overpressure: greater by σ in the case of borehole geometries and greater by 2σ for the spherical reservoir.

Addressing dry rock model critique. Guided by the first-order mathematics describing rupture of inflating boreholes and spherical reservoirs, it is now possible to assess the concerns that have been raised about the dry host rock model approach (Gudmundsson 2012).

Concern 1. The first concern is that dry rock tensile failure models include an 'extra' stress that is somehow superimposed upon (and hence violates) the lithostatic conditions in the host material, even though it has been demonstrated that dry rock models accurately reproduce lithostatic conditions (cf. Grosfils 2007, fig. 2a). Quantitatively, this criticism follows previous lines (e.g. Gudmundsson 1990, 2006) by defining the condition necessary for intrusion initiation from a fluid source, after adjusting signs to match the convention used in the numerical models, as

$$P_m = \sigma - T = \sigma + \Delta P \tag{11}$$

and hence, for failure, the overpressure required is

$$\Delta P = -T. \tag{12}$$

The assertion is that this criterion, which denotes failure of a pre-existing, internally pressurized, fluid-filled fracture (Jaeger & Cook 1979, section 17.5), describes both the initiation of hydraulic fractures injected from (vertical) drill holes as well as the overpressure required to fracture the wall of a magma reservoir and commence dyke injection (Gudmundsson 2012).

Comparing this assertion with the equations in the previous subsections, it is apparent that the criterion expressed in equation (12) is correct for a borehole only if the pore pressure in the host rock is assumed to be lithostatic in magnitude. [Note: the criterion is only approximately right (factor of 2 difference), given the same assumption, for a pressurized spherical magma reservoir.] If dry rock is instead employed for the host rock, the overpressure required becomes greater because the effective stress parallel to the borehole wall retains a magnitude of σ when inflation commences. Unlike the case when pore pressure is assumed to be lithostatic, in dry rock models the full wall-parallel components of the lithostatic stress continue to resist inflation-driven expansion and rupture. Contrary to the concern expressed, the difference between dry rock and 'overpressure only' model formulations is thus neither a result of adding an 'extra' wall stress to the former nor a violation of lithostatic conditions in the host rock. Instead, it simply reflects the fact that dry rock models include negligible pore pressure in the host rock, whereas 'overpressure only' formulations assume that the host rock has a lithostatic pore pressure and, thus, exists at the brink of tensile failure (see the subsection on 'Environmental parameters' later) prior to the initiation of magma reservoir inflation.

Concern 2. The second concern is that it is unreasonable to use $T = 0$ MPa (or a value close to it) for the host rock tensile strength. This value is often chosen in part for mathematical convenience (Grosfils 2007), but it also reflects the physical plausibility that any host rock mass will contain distributed fractures and, hence, will have little to no tensile strength (Zoback 2010, p. 121). Concern about this choice for T is an extension of Concern 1, for if equation (12) is used as the criterion for failure then only the tensile strength of the host rock is left to resist rupture. It follows that, if $T = 0$ MPa, nothing whatsoever resists rupture, and the slightest overpressure would cause the wall of a reservoir to fail (Gudmundsson 2012). Of course, this issue is not alleviated significantly if T remains small, of the order of a few MPa as is typical (Schultz 1995), since only slightly greater overpressures could be tolerated. In contrast, however, the failure criterion for dry rock retains the wall-parallel host rock lithostatic stresses (equation 7) because they have not been countered by lithostatic pore pressure. The wall-parallel lithostatic stresses also resist rupture and they are normally of much greater magnitude than T. As such, the decision to assume $T = 0$ MPa for convenience has a negligible effect on the deduced rupture characteristics (overpressure, location and fracture orientation; see Grosfils 2007, fig. 4). Thus, unless pore pressure is assumed to be lithostatic, this second concern is unwarranted. Using a low value for T is physically motivated, internally self-consistent and, furthermore, assuming any plausible value of T (including zero), has been demonstrated to have little to no impact on when/where a magma

reservoir in a dry host rock will rupture (cf. Grosfils 2007).

Concern 3. The third concern involves two separate parts that are again linked to and dependent upon the validity of Concern 1. The first part states that dry rock model formulations are faulty because they indicate that overpressures needed to induce rupture of a reservoir or borehole wall can become quite large at depth. This objection is not warranted in and of itself, of course, because, as discussed above, numerous laboratory experiments and borehole field measurements demonstrate that stress magnitudes P_m of approximately 2σ (equation 5) – that is, overpressures ΔP of around σ (equation 6) – are required for borehole hydraulic fracture in dry rock (e.g. Lockner & Byerlee 1977; Jaeger & Cook 1979). While the mathematics are not identical, the extension to magma chamber rupture and dyke injection is clear. The second part, which lies at the heart of the matter, is that the tensile strength of rock appears to be a material property that is effectively independent of confining pressure (i.e. depth). This is indisputable, but it is also irrelevant unless one assumes that pore pressure in the host rock is lithostatic in magnitude, as shown above, since, otherwise, the tensile strength is not the only factor resisting rupture. In the absence of pore pressure, the requirement of high overpressures to rupture the chamber wall, as is observed in borehole and laboratory equivalents, does not imply that the tensile strength must be greater than typical measured values (i.e. $T \leq 10$ MPa: Schultz 1995). The elevated pressure is required to overcome the combination of tensile strength and wall-parallel lithostatic stress (equations 6 & 7). The need for elevated overpressure does not indicate a flaw in the dry rock model formulation. It is, instead, a self-consistent outcome that does not contradict measurements of low tensile strength (as this factor is generally of minimal import among those resisting rupture in the absence of lithostatic pore pressure), and it is consistent with both laboratory and field data.

Summary. It is apparent that the 'overpressure only' and dry rock approaches are rooted in very different assumptions about the host rock conditions near a reservoir as it inflates towards failure. A traditional 'overpressure only' model formulation implies that the pore pressure in the host rock is lithostatic; that is, that the material surrounding the reservoir is in a state of incipient tensile failure at equilibrium. The implications of this assumption are that: (a) overpressure will rupture the reservoir wall once it is close to T in magnitude (with $T < 5$ MPa typical, implying that, at best, only minimal overpressure could ever develop); and (b) the tensile strength of the rock is the only thing resisting rupture as the reservoir wall expands. In dry rock models, however, no pore pressure is assumed. The implications of this decision are that: (a) the overpressure needed to cause rupture of the reservoir wall can become quite large at depth (although the magnitude required is sensitive to both reservoir aspect ratio and depth, and in many instances is fairly low: see 'Pressure for failure' for the subsections 'Uniform and layered half-space models' and 'Models with edifice loading' in the Results section of this paper); and (b) the tensile strength of the rock is of almost no importance when assessing reservoir rupture. Not only will the choice of pore pressure affect the magnitude of the overpressure required for rupture but, as described in the Results section below, there are other less obvious, yet equally important, volcanic implications – including the location and orientation of failure at the reservoir wall – that affect the geometry of the resulting intrusions and likelihood of surface eruption.

Results

While a great many volcanic scenarios and implications have been re-examined to date using a dry rock model formulation, we focus here on collating and summarizing three central outcomes: the overpressure needed to induce rupture; the location and style of initial failure; and the nature of the surface deformation that occurs in response to reservoir inflation. Each is an area critical to ongoing efforts to understand the nature of volcanic hazards on Earth, and each can provide important insight into the characteristics of volcanic activity on other bodies in the solar system.

Elastic models of magma reservoir pressurization tend to fall into two categories. In the first, the reservoir is treated as a point source (radius $\ll$depth), and, thus, the pressure and reservoir size are inseparable (e.g. Mogi 1958). This approach remains a powerful tool for modelling aspects of surface displacement, and continues to be widely used to gain insight into areas of active inflation (e.g. Rymer & Williams-Jones 2000; Newman *et al.* 2001, 2006; Pritchard & Simons 2004; Masterlark 2007; Parks *et al.* 2012). However, it also has considerable limitations (McTigue 1987), among which is an inability to model the stresses surrounding the reservoir – a critical factor since assessing the conditions for reservoir rupture in response to inflation is not possible. In the second category, mitigating these limitations, the reservoir is modelled as a finite, internally pressurized body within the lithosphere (e.g. Dieterich & Decker 1975). This is the approach the authors have employed when assessing magma reservoir inflation and

rupture as it permits explicit inclusion of free surface and similar effects, variable reservoir sizes and geometries, different host rock stress conditions, and a wide variety of other factors that can be introduced and examined systematically.

As reservoir inflation takes place in response to iterative increases in overpressure, stress magnitudes are monitored around the reservoir perimeter until tensile rupture occurs at the site along the wall where the failure criterion expressed in equation (7) is first met for either σ_t (wall parallel, in the rz-plane) or σ_θ (wall parallel, orthogonal to the rz-plane). Here we report this location using the angle α (Fig. 1), with $\alpha = 90^\circ$, $\alpha = 0^\circ$ and $\alpha = -90^\circ$ denoting the reservoir crest ($h = 0$ m), middle ($h = R_b$) and base ($h = 2R_b$), respectively. In some models, specifically those exploring ring faulting and caldera formation, the location and characteristics of Mohr–Coulomb failure are monitored and assessed in a similar fashion using the criteria defined in the subsection above on 'Reservoir failure criteria'.

Surface uplift and deformation has not been a primary focus of dry rock modelling efforts to date since their emphasis has been on constraining rupture characteristics, but limited assessments of uplift in half-space models have addressed two specific questions. First, how do the uplift predictions of Mogi (1958) compare with those obtained from numerical models when a uniform host rock is considered, and how do these results in turn compare with uplift expected when mechanical layering (i.e. strong and weak materials) is present? Second, do elastic models that invoke inflation to explain a given uplift event predict a stable reservoir, or is the pressure required greater than the rupture limit given the deduced reservoir geometry?

We begin here with an overview of several important insights obtained from dry rock half-space models. This baseline then informs a brief exploration of key differences observed and/or new findings obtained when additional factors such as edifice loading are introduced. Finally, we provide an initial report on the implications for ring faulting and caldera formation.

Uniform and layered half-space models

Pressure for failure. Using a simple half-space approach, with no surface topography but incorporating variable host rock density structures, Grosfils (2007) showed that the total uniform pressure ($\rho_r gD + \Delta P$) needed to induce rupture, when normalized to the lithostatic stress at the centre of a spherical reservoir (radius denoted simply as R when $R_a = R_b$), approaches a value of 3 for scaled reservoir depths R/DtC (where $DtC \equiv D + h$) approaching 0 (Fig. 2a). The choice to normalize by the lithostatic stress at the reservoir centre is useful when comparing an array of host rock density structures (not all of which vary linearly with depth), magma densities (neutrally buoyant and not), reservoir sizes and reservoir depths. The results show that the total uniform pressure needed for tensile rupture is insensitive to plausible density structures assumed for the host rock, the gravitational acceleration (g) employed and, for a given scaled depth, the reservoir radius.

For many applications, however, it is practical to isolate the overpressure needed for failure, and this is especially valuable for models in which the magma and host rock density are equal and uniform. Under these conditions normal stresses across the reservoir wall, once balanced at the reservoir crest, remain balanced with depth h below the crest. Since overpressure is defined here as the pressure in excess of lithostatic at the reservoir crest, in this type of depiction one typically normalizes the overpressure by the lithostatic stress at the crest. Recasting previously published data in this framework, the normalized overpressure magnitude is, as expected (see the subsection on 'Hydraulic fracture, dry rock'), effectively 2 for spherical reservoirs sufficiently distant from the free surface (Fig. 2b). Only when the reservoir lies at shallow depth ($D < R$), leading to stress modifications around the reservoir in response to considerable free surface displacement, does the overpressure required drop significantly. When compared with other reservoir geometries as well as simulations that include lithostatic pore pressure (Fig. 2c), the overpressure magnitude required to rupture a sphere at depth is the greatest, indicating that this geometry is normally the most stable (i.e. the most resistant to rupture) when responding elastically to overpressure-driven inflation. Although differences occur as the Young's modulus (E) for a uniform host rock is varied, reflecting the fact that the magnitude of surface displacement will increase in response to a given overpressure as Young's modulus decreases, scaled overpressure values varied on the order of 15% or less as E was changed across two orders of magnitude (1–100 GPa).

Many recent half-space studies have also examined the impact of mechanical layering in the host rock, implemented as Young's modulus variations that represent volcanic materials ranging from strong, coherent lava flows to weak ash layers (e.g. Trasatti *et al.* 2003; Gudmundsson 2006; Manconi *et al.* 2007, 2010; Trasatti *et al.* 2008). To examine how layering affects the scaled overpressure needed for rupture, models with a spherical reservoir of fixed radius ($R = 1$ km) are employed with the reservoir placed at different

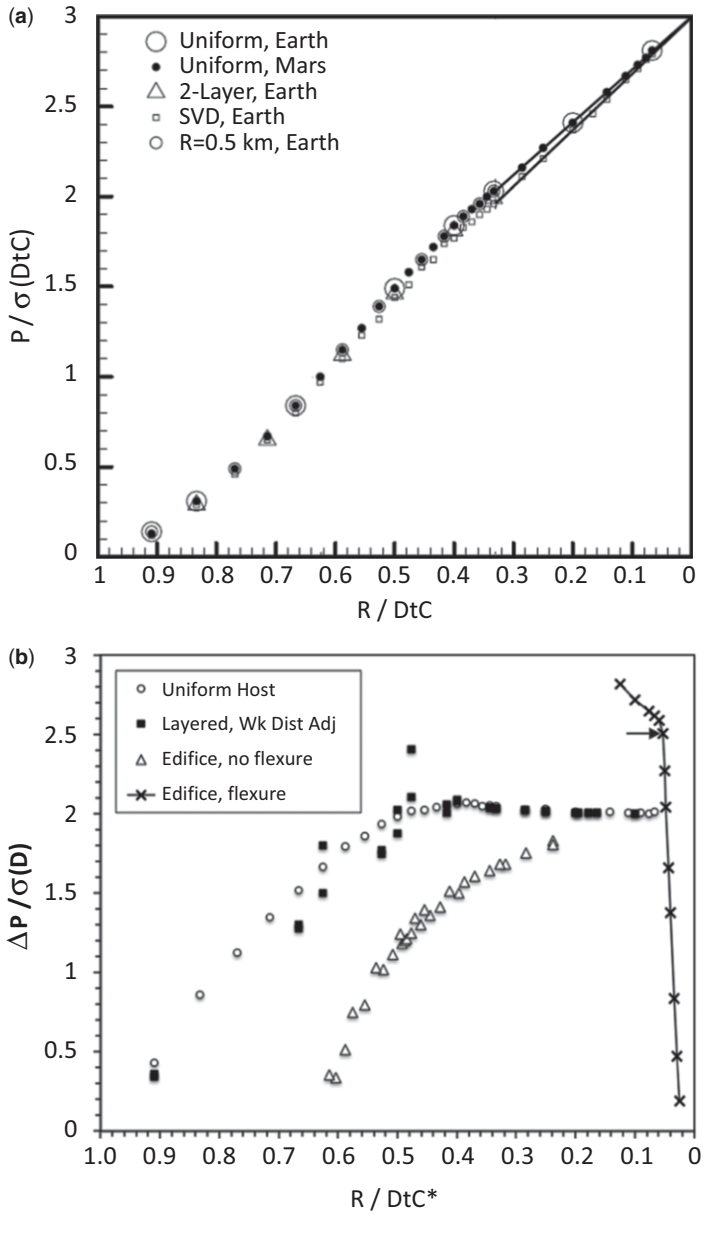

Fig. 2. Magma pressure required to induce tensile failure. (**a**) Uniform pressure P (sum in brackets from equation 1) required, normalized by the lithostatic stress at the depth of the reservoir centre (DtC), for a spherical reservoir as a function of scaled reservoir radius R. Tests of different host-rock density structures (uniform, two layer and smoothly varying (SVD)), gravity values (Earth, Mars) and reservoir radii (1 and 0.5 km) show that the uniform pressure is linearly dependent on the scaled radius but insensitive to the other parameters. From Grosfils (2007). (**b**) Magma overpressure ΔP required to induce rupture of a spherical reservoir, $R = 1$ km. The overpressure is normalized by the lithostatic stress at the top of the reservoir, while the radius is scaled by the distance between the reservoir centre and the nearest overlying weak layer, denoted for clarity by DtC^*. Uniform host rock data ($DtC^* = DtC$) are derived from (a). When $DtC > 2R$ then $\Delta P \approx 2\sigma_z(D)$, but at shallower depths the relative ΔP required drops precipitously. In layered models, DtC^* is the distance between the centre of the reservoir and the base of the nearest weak mechanical layer. For example, if the shallowest 500 m-thick near-surface mechanical layer is weak ($E = 1$ GPa) and the other is intermediate (like the host rock) or stronger, then $DtC^* = DtC - 500$ m. Proximity of the reservoir to a mechanically weak layer

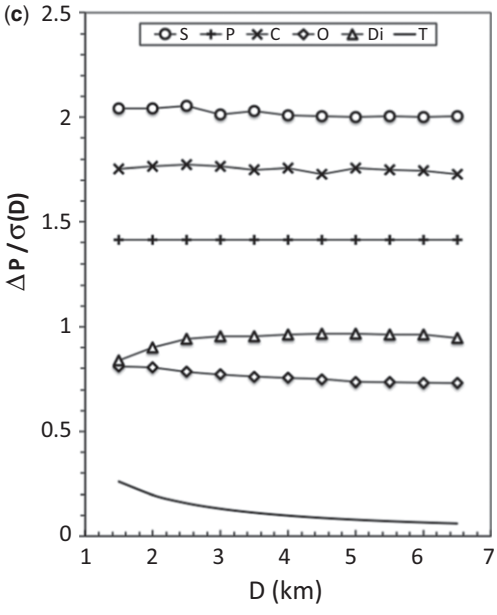

Fig. 2. (*Continued*) dictates ΔP in a fashion analogous to the uniform host rock case. Models of edifice ($V_h = 800$ m, $V_r = 77.2$ km) loading with a basal roller constraint exhibit a pattern similar to the uniform case for an edifice 800 m tall and 77.2 km in radius; here $DtC^* = DtC + 800$ m. The results demonstrate general resiliency; that is, no strong sensitivity to reservoir radius or depth. Models of edifice ($V_h = 5$ km, $V_r = 200$ km) loading with flexure ($T_e = 40$ km) exhibit very different behaviour: $DtC^* = DtC + 5$ km. Arrow denotes reservoir centred within the flexural neutral plane; at shallower depths, flexural compression makes failure increasingly difficult whereas, at greater depths, flexural extension sharply reduces the scaled overpressure required for rupture. (**c**) The importance of magma reservoir geometry, with all volumes identical to a sphere with $R = 1$ km. Range in D encompasses commonly inferred near-surface reservoir depths, avoiding free surface effects for the reference spherical geometry (S). Prolate (P) and cylindrical (C) reservoirs ($R_b = 1.25$ km) require progressively less overpressure to fail, while oblate (O) and discoidal (Di) reservoirs ($R_a = 1.25$ km) require less than half the overpressure needed to cause rupture of a sphere. Values depicted for non-spherical geometries are illustrative since greater elongation leads to higher stress concentration and lower overpressure. For comparison, (T) illustrates the results when a tensile strength of 5 MPa is the only thing resisting rupture (i.e. if pore pressure is lithostatic) of a spherical reservoir.

depths within host rock ($E = 60$ GPa) overlain by two 500 m-thick layers (Fig. 1), each of which is independently assigned a Young's modulus of either 1 GPa (weak), 60 GPa (control, host rock) or 100 GPa (stiff) magnitude (Long & Grosfils 2009). When the inflating reservoir is centred far below a mechanically weak material – either the free surface or a subsurface layer assigned a low Young's modulus – the scaled overpressure required for rupture hovers around 2 (Fig. 2b). As observed in uniform substrate models, however, the scaled overpressure declines rapidly as the distance between the reservoir and a weak overlying material layer decreases. In essence, reservoir wall displacement due to inflation occurs more readily when host rock deformation readily displaces a weak proximal layer, facilitating rupture (Long & Grosfils 2009). This first-order result indicates that a reservoir at depth will rupture at lower overpressure, when located near a weak subsurface layer, than when no weak subsurface layer is present. It is thus beneficial, when striving to understand the stability of an inflating magma reservoir, to incorporate as much knowledge of subsurface layering as possible into the model, especially since many studies also suggest that weak layers help magma reservoir formation by facilitating dyke–sill transitions (e.g. Gudmundsson 2006; Maccaferri *et al.* 2011). Further assessment, using reservoirs of different shapes and sizes as well as different subsurface materials, is needed to advance volcanologists' knowledge in this key area.

Location and orientation of failure. For a spherical reservoir, the location at which initial tensile rupture occurs, and the orientation of the resulting fracture, is sensitive to the scaled reservoir size and the host rock conditions assumed (Grosfils 2007). Since the lithostatic stress components parallel to the reservoir wall are of much less magnitude at the crest of the reservoir than at the base, inflation promotes rupture at the crest unless the reservoir lies very close to the surface, specifically when $DtC < 3R$ (Fig. 3a). When $DtC < 3R$, deformation of the free surface modifies the reservoir wall displacement, with greater displacement of the upper hemisphere shifting the point of failure away from the crest, closely tracking the relocation of the maximum strain deviation (Jaeger & Cook 1979) along the reservoir wall. When rupture takes place at the crest, $\sigma_t = \sigma_\theta$ and vertically ascending radial dykes will form whereas, away from the crest, σ_t reaches a state of tension before σ_θ and circumferential intrusion emplacement will initiate at the reservoir wall. In addition, because numerical models facilitate independent calculation of σ_t and σ_θ (normally only the latter is calculated in analytical treatments), rupture near the mid-point of the reservoir is now known to promote lateral sill emplacement (Grosfils 2007), not radial dyke injection, as is often assumed based on analytical model results (e.g. Parfitt *et al.* 1993; McLeod & Tait 1999).

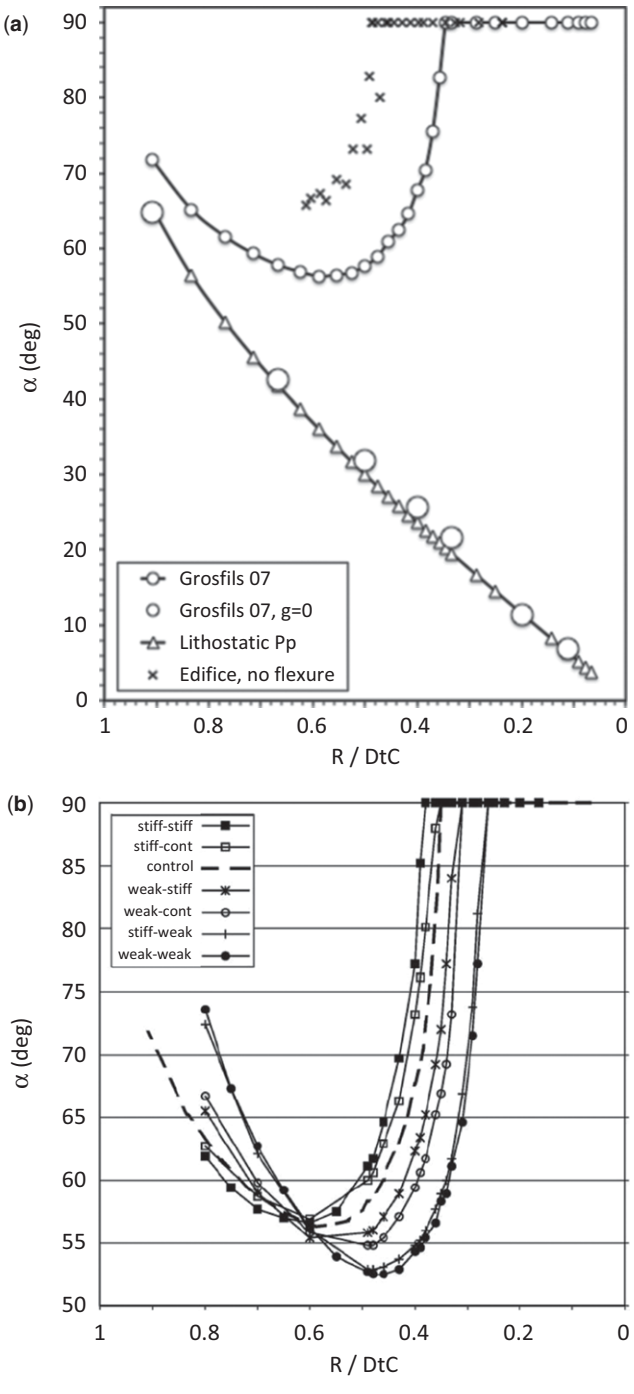

Fig. 3. Initial rupture location α. (**a**) Spherical reservoirs in a uniform host rock; edifice-loaded model matches conditions from Figure 2b. In dry rock models, $DtC > 3R$ promotes rupture at the crest, whereas failure rotates away from the crest for shallower reservoirs. Fracture orientation will initiate vertical dykes from the crest and circumferential intrusions elsewhere. 'Overpressure only' models (McTigue – lithostatic *P*p; numerical – Grosfils 07, $g = 0$) that account for the presence of the free surface exhibit a very different pattern of rupture. Modified from the original in Grosfils (2007). (**b**) Effect of mechanical layering implemented by varying Young's modulus.

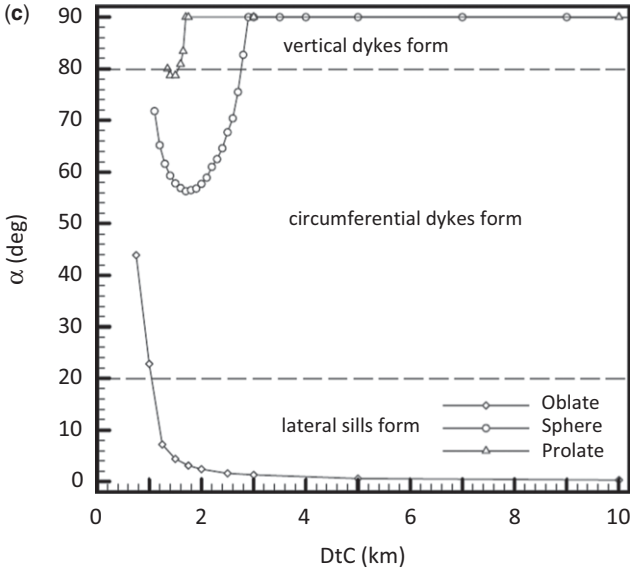

Fig. 3. (*Continued*) The legend lists a shallower layer then a deeper layer, weak is $E = 1$ GPa, control is $E = 60$ GPa (the same as the deeper host rock within which the reservoir lies), and strong is $E = 100$ GPa. 'Weak-stiff' thus denotes a configuration in which the shallowest mechanical later has $E = 1$ GPa, while the layer below this has $E = 100$ GPa; the host rock below has $E = 60$ GPa. For reference, the dashed line depicts uniform model results from (a). When $R/DtC < c.$ 0.6, the presence of strong layers above the reservoir shifts failure closer to the crest than in the uniform case, whereas weaker layers shift failure towards greater depth; the reverse pattern holds for reservoirs at shallower depths. In all models, initial fracture alignment will favour radial dykes at the crest and circumferential intrusions otherwise. From Long & Grosfils (2009). (**c**) Effect of geometry for spherical ($R = 1$ km), oblate ($R_a = 1.25$ km) and prolate ($R_b = 1.25$ km) reservoirs of equal volume. Compared to the spherical reference, stress concentration near the tip of a prolate reservoir pins rupture closer to the crest, whereas the same phenomenon pins rupture of an oblate reservoir to locations near *DtC* except at very shallow depth. Results shown are intended to be illustrative, as they depend on the degree of reservoir elongation. From Grosfils (2007).

The rupture location pattern observed in dry rock experiments is very different to the results predicted using 'overpressure only' model for mulations (Fig. 3a). Analytical models that take into account stress modifications caused by the free surface (e.g. Jeffrey 1921; McTigue 1987; Gudmundsson 1988; Parfitt *et al.* 1993) predict rupture near the *DtC* for a deep reservoir, with the rupture location occurring progressively closer to the crest for shallower reservoirs. If, in dry rock models, $g = 0$ m s^{-2}, this is equivalent to using a lithostatic pore pressure to establish an effective stress of 0 (both eliminate gravitational loading effects equivalently when assessing tensile failure), and duplicates the 'overpressure only' results. This demonstrates that dry rock numerical model formulations and those assuming a lithostatic pore pressure are, indeed, equivalent except for this key pore pressure difference, and underscores that the choice of host rock conditions sharply alters where rupture is expected to occur. It is interesting to note that, when lithostatic pore pressure is invoked, even if the top of a 1 km-radius reservoir lies within 100 m of the surface (i.e. $R/DtC = 0.9$) rupture cannot occur at the crest, and the circumferential intrusions emplaced will dip by approximately 65°. Intrusions initiated at deeper reservoirs will have shallower dips (Fig. 3a). Since vertical dyke ascent from reservoirs is a common element of many volcanic systems, the inability of the 'overpressure only' models to initiate vertical dykes argues against the validity of assuming lithostatic pore pressure in the host rock.

Mechanical layering in the host rock (Fig. 3b) yields the same approximate behaviour observed in the uniform half-space models (Long & Grosfils 2009). For a 1 km-radius spherical reservoir, as *DtC* decreases, the presence of two 500 m-thick weak (small *E*) layers at the surface above the reservoir means that deformation of the reservoir wall – and, hence, relocation of the point of failure – occurs more readily than in the control case and, thus, at greater scaled depth. Similarly, the presence of two stiff (high *E*) layers retards rotation of the point of failure away from the crest, so rupture will remain focused at the crest to

shallower scaled depths. Other configurations fall between these end-members. It is important to notice that, for *c.* $0.3 < R/DtC < c.$ 0.45 (if $R = 1$ km, $DtC = c.$ 2–3 km), the values of E selected for the shallow layers can have a significant effect on where rupture is predicted to occur. Thus, while the overarching behaviour resembles the uniform host rock case, incorporating known mechanical variations is of particular value when trying to assess where rupture of a very shallow reservoir, and intrusion, will commence.

As expected, failure location is also highly dependent on reservoir geometry (Fig. 3c). When compared with a spherical reservoir of equivalent volume, prolate reservoirs concentrate stress at their upper and lower tips, and so are less perturbed by the presence of the free surface. As a result, they continue to rupture at the crest when centred at much shallower depths. Similarly, owing to stress concentration at the lateral tips, an oblate reservoir will rupture near the *DtC* unless it lies very close to the free surface. In this instance, stress modifications caused by the free surface deformation will rotate the point of failure towards the crest. However, even at the shallowest depth depicted in Figure 3c, the failure location has only rotated halfway to the peak.

Surface deformation. Modern measurement of surface displacement using GPS (Global Positioning System), InSAR (Interferometric Synthetic Aperture Radar) and other techniques remains a valuable tool for gaining insight into the inflation (or deflation) of a subsurface magma body (e.g. Owen *et al.* 1995, 2000; Cervelli *et al.* 2001; Bartel *et al.* 2003; Dzurisin 2003; Pritchard & Simons 2004); while discussion focuses here on vertical displacement, simultaneous assessment of radial displacement data provides clearer insight into the magma body than vertical displacements alone (e.g. Newman *et al.* 2001, 2006; Battaglia *et al.* 2003; Sturkell *et al.* 2008). Analytical point source models can duplicate observations readily (e.g. Mogi 1958), leading to estimates of volume change at depth, while analytical models of finite cavity inflation permit more direct insight into overpressure variations and analysis of shallow reservoirs (e.g. Davis 1986; McTigue 1987). For instance, using a spherical reservoir of radius $R = 1$ km and $DtC = 5$ km in a uniform host rock with $E = 60$ GPa, the uplift predicted for an overpressure of 10 MPa using analytical models is just over 12.5 mm (Fig. 4a); as Young's modulus increases, displacement magnitude decreases. Setting $g = 0$ m s^{-2} in dry rock numerical models, equivalent in outcome for these purposes to assuming the pore pressure is lithostatic, the uplift predicted is almost identical to (0.25 mm lower than) the analytical benchmark. To match the analytical uplift requires increasing the overpressure by 0.15 MPa or decreasing the depth by 50 m, indicating an error of 1–2%. If, instead, a dry rock host is used, the overpressure required to produce the same uplift is 112.1 MPa. This is, however, simply the lithostatic pressure at the crest (*c.* 102 MPa) plus the 10 MPa overpressure, once again demonstrating the equivalency of the two sets of mathematics. What is different, however, is the reservoir's proximity to failure. In the 'overpressure only' (lithostatic pore pressure) models, assuming a standard tensile strength value of approximately 5 MPa for the host rock, rupture of the reservoir will either have occurred or be imminent under the model conditions described. This implies that the maximum uplift that can occur prior to rupture is surprisingly small, of the order of 12 mm. In contrast, equivalent models assuming dry rock yield the same sort of radially decaying profile but permit just over 250 mm prior to rupture initiation (Fig. 4a).

Half-space models of uplift (described in 'Pressure for failure' in the subsection 'Uniform and layered half-space models' in the Results section) that incorporate shallow mechanical layers (e.g. Long & Grosfils 2009) demonstrate how surface displacements can vary significantly depending upon the Young's moduli (E) values assigned to them (Fig. 4b), a result that is consistent with the inverse relationship between Young's modulus and displacement. When compared with the control case (both near-surface layers assigned the same E as the host rock), the use instead of stiffer layers tends to reduce uplift above an inflating sphere, while weaker layers have the opposite effect. In addition, when equivalent volume oblate and prolate reservoirs are examined, oblate reservoirs induce more inflation than the spherical case, while prolate reservoirs induce less. A more comprehensive discussion of uplift patterns, the relationship to subsurface strain within a weak layer and other factors is provided by Long & Grosfils (2009), but two first-order points are worth calling attention to here. First, even with the multiplicative factors added by using oblate reservoirs and weak surface layers, 'overpressure only' elastic models are generally incapable of producing commonly observed degrees of uplift without invoking overpressures much greater than those required to induce rupture (e.g. Grosfils 2007; Long & Grosfils 2009). Second, future measurements of surface uplift on Venus or other planets using InSAR-like techniques will be tremendously useful for identifying centres of active magmatism. However, inferring volcanological conditions with confidence requires more detailed knowledge of the subsurface geology than is currently available for many centres of activity on Earth, let alone the other bodies in our solar system.

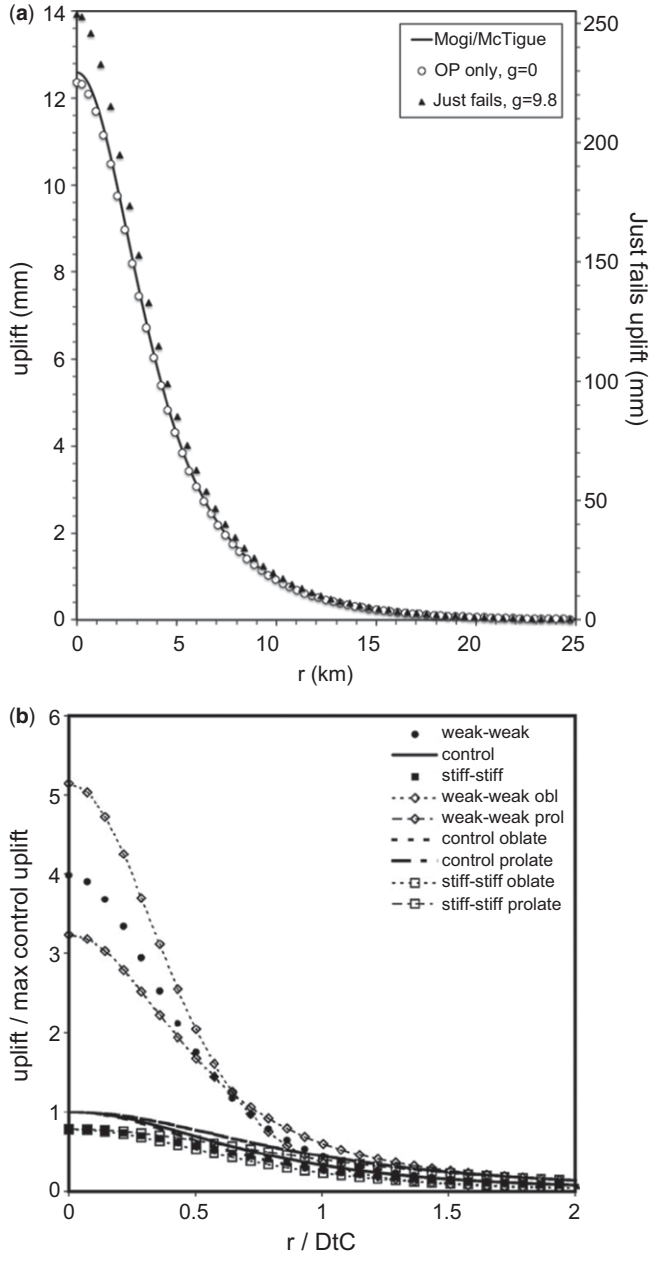

Fig. 4. Surface uplift above an inflating magma reservoir. (**a**) Spherical reservoir; $R = 1$ km, $DtC = 5$ km, $\Delta P = 10$ MPa. The Mogi–McTigue solution is closely matched by 'overpressure only' models. The same uplift profile (not shown) is obtained from a dry rock model, $g = 9.8$ m s^{-2}, when uniform pressure $P = 112.1$ MPa; this is simply the lithostatic load at the crest (102 MPa) plus the same 10 MPa overpressure. In the 'overpressure only' model, approximately 12.5 mm is the maximum uplift the system can sustain before rupture, well below magnitudes commonly observed. However, about 250 mm of uplift can occur prior to rupture in the dry rock model, which more closely resembles measurements from actively inflating volcanic systems. Modified from Grosfils (2007). (**b**) Effects of mechanical layering and reservoir geometry variations within the host rock; the protocol for layer stiffnesses and configuration follows Figure 3b. Weak layers at the surface promote significantly greater uplift, while stiffer layers decrease uplift magnitude. When compared with a sphere, these effects are amplified for oblate reservoirs and depressed when a prolate geometry is employed instead. Original from Long & Grosfils (2009).

Models with edifice loading

Pressure for failure. The overpressure required to rupture a spherical reservoir beneath a conical surface load, a geometry considered a good approximation of a typical edifice (Grosse *et al.* 2009), will depend on the size and shape of the edifice, and the volume (V) relative to that of the reservoir (Pinel & Jaupart 2000; Hurwitz *et al.* 2009). An illustration, using an intermediate-sized Venusian edifice (volcano height $V_h = 0.8$ km, volcano radius $V_r = 77.2$ km), is shown in Figure 2b. For an array of reservoir size–depth combinations, addition of the edifice load decreases the overpressure markedly relative to the half-space model results, but the general pattern is otherwise quite similar. In contrast, when flexural effects are added to the model, the rupture behaviour is quite different (Galgana *et al.* 2011). Flexural stresses created by a surface load create an hourglass pattern in which depths above and below a flexural neutral plane (low differential stress) are subjected to increasing compression or extension, respectively (see also McGovern *et al.* 2013). To illustrate the impact this has on the overpressure needed for reservoir rupture, data from a model of a large Venusian edifice in a region of high elastic thickness ($V_h = 5$ km, $V_r = 200$ km and elastic thickness $T_e = 40$ km) are plotted in Figure 2b; all data are for a spherical reservoir with $R = 1$ km. Even at the neutral plane (*c.* 14 km depth: Galgana *et al.* 2011), the overpressure needed for rupture is considerably higher than in the half-space models or in models that include an edifice but not flexural adjustments. At shallower depths, as the reservoir moves increasingly towards the surface and into areas of greater flexural compression, the overpressure needed also increases. At greater depths the reverse is true: as the reservoir moves away from the neutral plane and into areas of greater flexural extension, the overpressure drops precipitously, reaching levels comparable to those otherwise achieved only at very shallow scaled depths in half-space models.

Location and orientation of failure. When compared to half-space conditions, the weight of an edifice tends to amplify the expected reservoir rupture patterns (Hurwitz *et al.* 2009). For instance, as shown in Figure 3a, the presence of an edifice pins rupture to the crest of a spherical reservoir unless it is located at very shallow depth, in which case the rupture location is rotated away from the crest by the deformation induced at the free surface. Similar patterns are observed for non-spherical reservoirs. Regardless of reservoir shape, these effects are stronger for steeper stratocone-like edifices (with more mass concentrated near the rotation axis) than for shield-like volcanoes, and larger reservoirs require larger edifices to have the same impact. As in the half-space models, failure occurs in the σ_t orientation for these edifice-loaded simulations, initiating vertical dykes at the crest, lateral sills near the mid-section, or inclined circumferential intrusions in-between.

When flexure in response to the edifice load is introduced, the rupture patterns are dominated by the resulting hourglass stress state in the lithosphere (Galgana *et al.* 2011). Near the neutral plane, where differential stresses are low, the reservoir behaves as if it were simply located at great depth in a half-space, failing at or near the crest. At greater depths, the least compressive stress is horizontal and, thus, reservoirs will fail at either the crest or the base depending on the balance of effects stemming from their distance below the free surface (which favours failure at the crest) and the depth-dependence of the differential stress increase (which favours failure at the base). Above the neutral plane, the least compressive stress is vertical, and reservoirs will, therefore, fail at or just above their centres to feed lateral sills.

Taking into account both pressure and rupture location data, it is instructive to now examine the differences between equivalent dry rock (Hurwitz *et al.* 2009) and 'overpressure only' (Pinel & Jaupart 2003) models when an edifice load is present (Fig. 5). For this simulation, following Pinel & Jaupart (2003), $R = 4$ km, $DtC = 5$ km, $V_h = 0.4$ km, $V_r = 4$ km and $T = 20$ MPa. Using dry rock models, inflation of the reservoir (thin line defined by the arrows showing displacement, exaggerated 1500× in the figure for clarity) causes initial rupture and circumferential intrusion at $\alpha = 58.9^\circ$ when $\Delta P = 58.5$ MPa (full grey circle). If gravitational effects are eliminated in the host rock to simulate the existence of lithostatic pore pressure, leaving just the overpressure loading the reservoir and the edifice weight applied at the surface, the resulting displacement is the same, demonstrating the equivalence of the two models in this regard. However, because only the tensile strength resists rupture in this case, application of this overpressure magnitude would cause the entire wall to rupture in tension (thick grey line). If the overpressure magnitude is reduced sufficiently, to $\Delta P = 21.2$ MPa, the conditions defining initial failure in an 'overpressure only' formulation are identified, with rupture occurring instead at $\alpha = 90^\circ$ to feed a vertical dyke (half grey circle). This example illustrates that, even though equivalent overpressures will produce equivalent displacements, not only will the overpressure magnitude needed for initial rupture differ substantially in the two model formulations, as discussed in the section on 'Uniform and layered half-space models', but as a result the location of

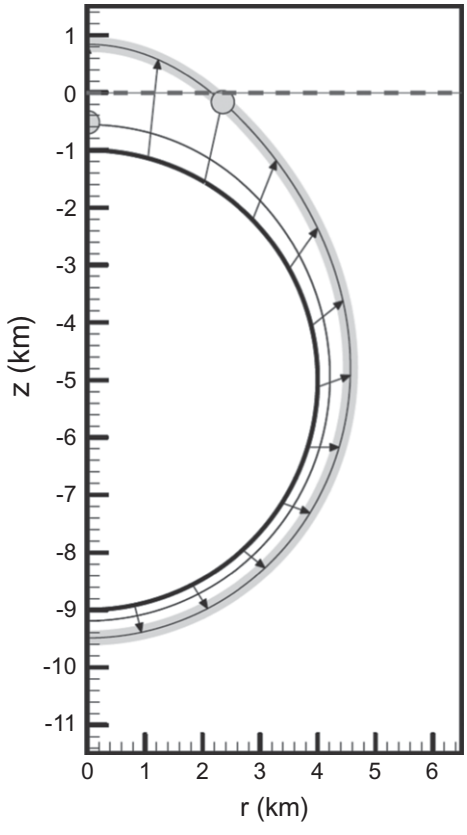

Fig. 5. Comparison of deformation rupture conditions for a spherical reservoir inflated to the point of failure under dry rock and 'overpressure only' host-rock conditions beneath a small conical edifice ($V_h = 400$ m, $V_r = 4$ km). Arrows denote displacement (1500×) resulting from inflation to the point of failure in dry rock, which occurs at $\alpha = 58.9^\circ$ (small grey circle on the outer black line). In 'overpressure only' models, inflated at the same ΔP, identical displacement occurs, but under these conditions failure happens along the entire reservoir margin (thick grey line). Reducing ΔP until the point of first failure occurs, displacement is greatly reduced and $\alpha = 90^\circ$ (half grey circle, on inner black line). In both models, the impact of the small edifice is evident but, when comparing them both, the displacement and the location of failure differ when conditions promoting initial rupture are implemented. From Hurwitz *et al.* (2009).

failure and style of intrusion can vary significantly as well.

Surface deformation. As noted previously, our emphasis has been on elucidating the conditions needed to initiate rupture of a subsurface reservoir. Surface deformation is challenging to interpret volcanologically, even in simple half-space models (see 'Surface deformation' in the subsection on 'Uniform and layered half-space models'), and we are not aware that any systematic parameterized study conducted to date has examined the interplay between edifice loading, reservoir inflation and the resulting patterns of surface deformation. This may be sensible given that additional components like mechanical layering (e.g. Manconi *et al.* 2007, 2010) should also be included if one wishes to deduce subsurface magmatic conditions from observed surface deformation. Instead, researchers have focused their efforts on matching uplift patterns at specific volcanoes where abundant independent constraints on the subsurface host rock geology exist (e.g. Currenti *et al.* 2010; Ronchin *et al.* 2013). Such endeavours can provide powerful insight into a specific edifice or situation when the models are formulated carefully. As noted immediately above, the pressures deduced and failure patterns expected will depend quite sensitively on the host rock conditions employed and, since overpressure magnitude is directly linked to both displacement (observed) and rupture (limiting condition), it is critical to verify that the magma reservoir overpressure conditions inferred from displacement modelling do not violate the rupture constraints for the system under study (cf. the discussion of Long Valley inversions: Long & Grosfils 2009).

Ring fault initiation

While the sections above focus on tensile failure of an inflating reservoir, under normal conditions shear failure will occur first (e.g. Gerbault 2012). The extent to which shear failure affects the inflation process by promoting reservoir-fed intrusion remains poorly understood, and more careful future analysis is required to assess this problem. However, it is certain that shear failure and fault slip are necessary elements of ring faulting and caldera formation, and that caldera formation can be accompanied by massive and devastating eruptions.

To better understand how ring faulting initiates above a magma reservoir in response to inflation, basic volcano-tectonic conditions conducive to ring fault formation have been proposed as numerical modelling constraints (cf. Gudmundsson 1998; Folch & Marti 2004). The crux is that ring fault formation is argued to occur when conditions promote the development of (1) steeply inclined normal faults that (2) propagate downwards from regions of maximum tensile stress at the surface and (3) link up with a region of high shear stress at the outer margins of the reservoir. This combination is difficult to create and, therefore, is in conceptual agreement with the observation that slip

on caldera-bounding faults occurs only rarely in active systems (Newhall & Dzurisin 1988). The proposed conditions are useful constraints, but there is concern because: (1) in formulating the link between magma reservoir pressure variations and failure in the host rock, models often adopt conditions that imply lithostatic pore pressure, which is not known to be a pervasive effect above shallow, caldera-forming reservoirs; (2) the approach assumes fault behaviour (e.g. geometry and point of origin) that is restrictive given the diverse range of field observations available to constrain fault attitude and, to a limited extent, propagation direction (Geshi *et al.* 2002; Marti *et al.* 2008); and (3) results obtained are different to those from analogue models – which, for instance, predict outwards-dipping ring faults that grow upwards from the reservoir – even when similar circumstances are examined. The latter concern has led many numerical modellers to question the applicability of physical simulations (e.g. Gudmundsson 2007), but it should also undermine confidence in the validity of existing numerical results (Acocella 2008) until agreement between the two approaches can be demonstrated.

The dry rock modelling approach avoids the first two assumptions, letting the model system mechanics dictate the conditions for fault initiation and geometry, and detailed exploration of how evolution of an inflating magmatic system can prime the host rock for ring fault formation is underway. As in the models described in previous sections, stresses parallel to the reservoir wall are monitored for tensile failure. In addition, Mohr–Coulomb failure criteria (cohesion of 10 MPa and angle of internal friction set to 25°) and parameterized Andersonian stress states linked to fault type (Simpson 1997) are used to assess the potential for, and alignment of, shear failure. While this effort remains a work in progress, the basic approach is demonstrated here using a discoidal reservoir subjected to overpressure conditions (Fig. 6). This example duplicates a geometry modelled previously using 'overpressure only' conditions for which it was concluded that 'the maximum tensile and shear stress both occur at a point directly above the centre of the chamber and (conditions) are thus not favourable to ring-fault formation' (Gudmundsson 2007, p. 155).

When overpressurized to the point of initial tensile failure (Fig. 6), assumed here to be the maximum inflation a reservoir will undergo prior to relieving the pressure via intrusion, Mohr–Coulomb failure within the host rock occurs across a broad zone at the surface and along the outer edge of the discoidal reservoir. Above the roof of the reservoir (green shades), stress tensor conditions favour the formation of normal faults according to Andersonian criteria, but examination of optimal concentric Mohr–Coulomb failure plane orientations reveals that Mohr–Coulomb failure permitting ring fault subsidence in this area will require reverse slip. Thus, alignment of the slip planes and the faulting style required by the stress state are in conflict, and ring fault initiation and subsidence during inflation will be very difficult. Beyond the lateral extent of the reservoir (red shades), a similar mismatch between the stress conditions and Mohr–Coulomb failure plane alignments should prevent ring fault initiation and subsidence. Critically, shear rupture will first occur at the reservoir wall within this zone at $h \cong 500$ m but, because conditions do not favour ring fault growth or subsidence at this location, local fault adjustments should dominate the response within the host material. This is consistent with earthquake data from active magmatic centres, and we hypothesize that ruptures remaining local in extent will generally modulate neither the reservoir pressure nor the structural evolution significantly. Put another way, the host rock will adjust locally but, unless volumetrically significant intrusion occurs, inflation will continue and the area of Mohr–Coulomb failure will continue to expand until either conditions favour larger, throughgoing faults or tensile rupture occurs.

Between the two extensive regions where ring fault initiation and subsidence appear to be prohibitively difficult there is a narrow, near-vertical zone above the margin of the reservoir where the sense of fault slip and alignment of the Mohr–Coulomb failure planes match. These planes are anchored in an area of Mohr-Coulomb failure, and shear faulting at this site is expected somewhat before tensile failure. The host rock between the nucleation site at the reservoir and the surface has not generally exceeded the Mohr–Coulomb failure limit, raising questions about whether or not a throughgoing ring fault is possible prior to tensile failure, but the conditions are otherwise primed, mechanically, for ring faults to form: the faults can initiate, the stress conditions in the host rock are amenable and alignment of the most likely slip planes is suitable. Stresses associated with dynamic crack growth, or other factors not captured in static continuum models, are likely to play a key role in determining when caldera-like ring faults will be produced, and advancing models that incorporate such factors (cf. Holohan *et al.* 2007; Gerbault 2012) will probably expand the understanding of caldera formation appreciably.

As is true of other ring-faulting assessments, dry rock numerical models help evaluate when conditions are suitable and unsuitable for this type of structure to form. For the example described here, suitable ring-faulting conditions are established readily and without invoking special external

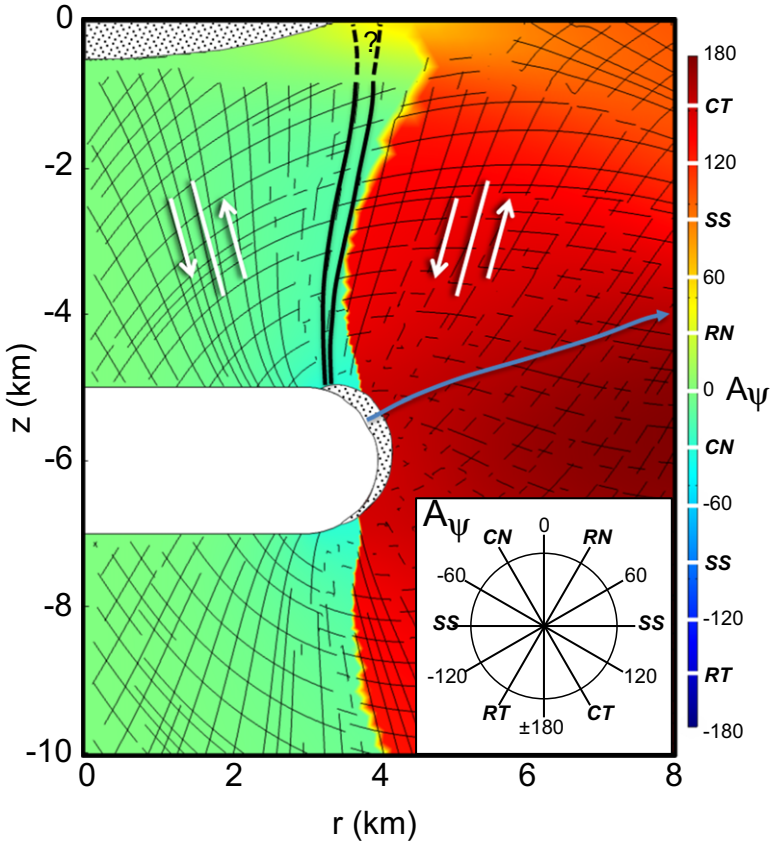

Fig. 6. Illustration of shear rupture failure model and interpretation. Inset depicts the A_ψ parameter (Simpson 1997) for Andersonian faulting; RN, pure radial normal; CN, pure concentric normal; RT, pure radial thrust; CT, pure concentric thrust; SS, pure strike-slip. In this dry rock model with a discoidal reservoir, stress conditions needed to initiate tensile rupture with $T = 5$ MPa are depicted; the path for the sill that would originate just above the mid-depth and relieve overpressure is denoted by a blue arrow – no eruption is expected. Well before tensile rupture occurs, zones of Mohr–Coulomb failure (white stippled pattern) form first at the surface (starting at $r = 0$ km) and then at the reservoir wall (starting along the upper edge at $r = 3.85$ km). Thin black lines show orientations of conjugate Mohr–Coulomb slip planes ($C = 25$ MPa, $\phi = 25^\circ$), plotted only where the planes are concentric; the steep set above the reservoir resembles ring fault geometries observed in the field, while the other does not. Ring fault initiation and caldera subsidence is possible in regions where the A_ψ fault type (colour) and sense of slip needed for ring faulting and caldera subsidence (see white arrows) agree, provided that spatial overlap with a zone of Mohr–Coulomb failure also occurs. A narrow zone at the reservoir margin (thick black lines) meets these conditions and is thus primed for ring fault formation.

continuum conditions such as regional extension or domal uplift, a finding contrary to results reported based on an 'overpressure only' model formulation (Gudmundsson 2007). In addition, while further discussion is not pursued here, a dry host rock model approach accurately duplicates published analogue model results that simulate underpressure conditions (Kennedy *et al.* 2004), providing a new mechanical basis for understanding why initial outwards-dipping ring faults jump laterally to form steep, secondary, inwards-dipping faults (Grosfils 2011).

Discussion

In the Results, we reported several key results from dry rock modelling efforts to date. Below, we draw on these data to summarize why such models are suitable for analysing volcanism in diverse settings before exploring some implications for several types of reservoir-derived volcanic features commonly found on the terrestrial planets. We conclude with a brief discussion of elastic model limitations, and by framing a set of key directions that will benefit from additional future research.

Environmental parameters

Finite element numerical models exploring magma reservoir mechanics are an excellent tool for assessing this aspect of volcanism in a planetary context. Magma and rock characteristics, such as density and strength, which derive from material properties that are invariant (i.e. the tensile strength of a given basalt does not depend on the planet where the basalt is found), are not expected to affect model applicability to different planetary contexts. Similarly, while not discussed at length in the current contribution, neither plausible host rock density structures nor magma density variations play a major role in defining the location or conditions of tensile rupture unless the lithostatic stress is negated (Grosfils 2007), for instance by lithostatic pore pressure. The interplay between density variations will, of course, affect dyke propagation significantly and, with other factors, helps to dictate the depth at which a magma reservoir will form on a given planet (e.g. Wilson & Head 1994).

When inflation drives a reservoir to the point of tensile rupture, the scaled overpressure required is identical whether the gravity of Earth or Mars is employed in the model (Fig. 2), demonstrating that the mechanical response is independent of the planetary gravity applied. While gravity will, in part, dictate the atmospheric pressure applied to the surface, a factor neglected in the model results reported here, as pressure increases (e.g. for Venus) this is equivalent to the reservoir behaving as if it resided at slightly greater depth. However, even for Venus, this is comparable to only a few hundred metres of extra overburden, which does not meaningfully affect the results reported here. Gravity's impact on shear rupture conditions has not yet been assessed systematically, but depth-dependent variations are expected to occur because the depth needed to achieve a given normal stress across a fault (equation 2) will depend on the magnitude of the gravitational acceleration (see the subsection on 'Caldera formation' in the 'Discussion' section).

Critically, it is clear from comparing recent dry rock with traditional 'overpressure only' simulations that the host rock stress state environment assumed becomes a key factor when evaluating the evolution and rupture of a magma system at depth. 'Overpressure only' elastic models imply lithostatic pore pressures in the host rock (see the earlier subsection on 'Hydraulic fracture, elevated pore pressure'). Use of lithostatic pore pressure implies that the effective stress in the host rock ($\sigma - P_p$) is 0 (Hubbert & Rubey 1959; Gerbault 2012); that is, that the entire rock mass must exist in a state close to tensile failure even at equilibrium. This is contrary to what is normally observed even in critically stressed crust (Zoback 2010), although clear exceptions exist (Engelder & Leftwich 1997). Even when ideal conditions occur, however, establishing and maintaining lithostatic pore pressures at shallow, reservoir-hosting depths is believed to be difficult in most geological settings (Brace 1980; Nur & Walder 1990; Swarbrick & Osborne 1998; Simpson 2001; Zoback 2010). Because pore pressures (a) vary widely on Earth and are temporally and spatially variable, (b) are unknown for most active and relict volcanic systems, and (c) are difficult to achieve and sustain at lithostatic values over time, we argue that dry rock models represent an appropriately conservative and logically defensible end-member to use for establishing a baseline on which to build when exploring volcanic system characteristics. This is even more true when considering volcanism in a planetary context, as the dry rock model formulation is not only the most obvious choice for targets such as Venus, where pore fluids that weaken rock are unlikely to exist at shallow depth owing to elevated temperature, but also the best starting point to use for bodies such as Mars where pore pressure of some kind is plausible but unconstrained in magnitude (e.g. Kohlstedt & Mackwell 2010). Key differences between the models, when compared with observations, have several important volcanological implications, summarized below. Observations are generally, although not uniformly, better matched by dry rock model formulations and results.

First, in 'overpressure only' models, rupture of a spherical reservoir wall is resisted solely by the tensile strength of the material (equation 10). With $T \leq 10$ MPa, but normally only 2–3 MPa (Schultz 1995), overpressures of the order of approximately 5 MPa are sufficient to cause rupture, and 20 MPa (*c.* $2\,T$) becomes the effective limit of what a reservoir can sustain prior to failure. Even if one ignores pressure increases derived from infusion of new material, known to be a common occurrence and a factor that often triggers eruption, 5 MPa is very low given pressures expected from small amounts of crystallization alone (Tait *et al.* 1989). The implication is that reservoirs of plausible sizes should fail almost immediately either when new magma is injected or shortly after crystallization commences. In contrast, dry rock models require constant scaled overpressures to rupture reservoirs at low R/DtC ratios (Fig. 2), but the magnitude of the overpressure needed decreases significantly at shallower depths or in response to variations in surface loading conditions and/or reservoir geometry. To illustrate, a spherical reservoir in a uniform half-space with $R = 1$ km and $DtC = 3$ km requires $\Delta P = 102$ MPa to rupture (i.e. for $\rho_r = 2600$ kg m^{-3}, the lithostatic load on Earth at $D = 2$ km is 51 MPa), whereas the

same reservoir with $DtC = 1.75$ km requires only $\Delta P = 34$ MPa, or $\Delta P = 10$ MPa when located beneath an intermediate-sized edifice (Fig. 2b). A mildly oblate reservoir of equivalent volume in a uniform half-space will fail at small R/DtC when $\Delta P <$ *c.* 40 MPa (Fig. 2c). These examples demonstrate that overpressures needed to induce failure of reservoirs in dry rock models at commonly inferred reservoir depths can often be quite reasonable. In addition, for a reservoir at a given DtC, increasing R means that the overpressure required to induce failure decreases. If small reservoirs form at depth, they will require fairly high overpressures to rupture given the magnitude of the lithostatic stress resisting failure. Instead, they have the opportunity to expand stably in response to magma influx (e.g. Jellinek & DePaolo 2003). Ultimately, the R/DtC scaling places a depth- and geometry-dependent limit on the reservoir size that can be achieved before rupture occurs.

Second, in 'overpressure only' models, deep-seated spherical reservoirs will fail near their mid-depth, feeding sills (radial dykes are not predicted: Grosfils 2007), while reservoirs at increasingly shallow depths will feed circumferential intrusions with increasingly steep dips (Fig. 3). Deep reservoirs will, therefore, stabilize in place through lateral intrusion and elongation, without feeding magma regularly to shallower depths. Indeed, contrary to what is commonly observed, vertical dyke injection from the crest and direct vertical magma ascent is not strictly possible. Because the effective stress in the host rock is zero, however, differences between the host rock and magma densities can help dictate the failure location (Pinel & Jaupart 2000); if a layer of sufficient thickness accumulates at the top of the reservoir, then rupture nearer the crest can occur, for instance, but for basalts at least sufficient foam accumulation is difficult to achieve under normal magmatic conditions (Parfitt *et al.* 1993). In contrast, for dry host rock conditions, deep-seated spherical reservoirs will rupture near the crest and feed magma to shallower depths while, at shallow depths, the failure location rotates away from the crest and reservoirs will emplace circumferential intrusions (Fig. 3). Edifice loading will pin the rupture location more firmly to the crest, mechanical layering plays, at most, a limited role and only oblate reservoirs at depth will stabilize in isolation from the surface; that is, without promoting magma ascent upon rupture.

Third, limits placed on the overpressure by rupture conditions also limit the surface deformation that can occur. Uplift magnitude will depend on the stiffness of the host rock and the effects of mechanical layering (cf. Long & Grosfils 2009; Geyer & Gottsmann 2010), but values of a few centimetres are expected for typical reservoir geometries and mechanical layering configurations in 'overpressure only' models (Fig. 4). In essence, any small increase in magma overpressure should lead readily to intrusion. Hence, inflation could drive only minimal surface uplift before the pressure is relieved (see 'Surface deformation' in the subsection on 'Uniform and layered half-space models'), a result that is inconsistent with observations of considerable surface inflation, as well as low intrusion frequencies during inflation events at active magmatic centres world-wide (e.g. Newhall & Dzurisin 1988; Pritchard & Simons 2004; Chaussard & Amelung 2012). Dry rock models, however, permit considerable uplift that, for otherwise identical conditions, is an order of magnitude or so greater than in the 'overpressure only' formulations (Fig. 4). This result is in better agreement with the decimetre- to metre-scale displacements commonly measured in volcanically active areas (Berrino *et al.* 1984; Pritchard & Simons 2004; Gottsmann *et al.* 2006; Baker & Amelung 2012; Chaussard & Amelung 2012), and intrusion frequency will be lower than in 'overpressure only' models because rupture is more difficult. Even with these much greater values, however, uplifts such as the 1.5 m observed at Campi Flegrei in 1982–1984 (Berrino *et al.* 1984) are not easily explained using an elastic model alone (Trassati *et al.* 2005; Grosfils 2007), indicating that alternative rheologies or factors must be considered. It is worth noting as well that caution is required when using elastic 'overpressure only' models to infer reservoir conditions from surface inflation events. While excellent fits can be achieved (e.g. Battaglia *et al.* 2003), the pressures invoked are sometimes well in excess of the limit placed by tensile rupture for the reservoir geometries employed. This indicates that rupture criteria should be used jointly with surface deformation inversions when striving to constrain the depth, geometry and overpressure present within an actively inflating magma reservoir (Long & Grosfils 2009).

Implications for reservoir-related planetary volcanism

Finite element models examining magma inflation and rupture typically assume that the reservoir wall has no unusual stress-concentrating defects, but local inhomogeneities are, of course, likely to alter the nature of the failure process by introducing irregular stress concentrations that are difficult to model (e.g. Letourneur *et al.* 2008). The key question is, however, do such inhomogeneities play a critical role? Field observations – for instance,

persistent emplacement of radial intrusions linked to shallow magma sources – indicate that reservoir inflation and rupture repeatedly produce remarkably similar volcanic landforms across a wide range of scales and geological settings. This implies that observed patterns of magma reservoir volcanism are not generally dictated by local inhomogeneities, and that they, instead, derive from overarching factors that are predictable and linked to the inflation process and response. Idealized analysis of wall-parallel stress magnitudes (cf. Russo *et al.* 1997) using numerical models is thus expected to provide useful insight into the nature of reservoir rupture, and any corresponding magmatic and/or volcanic activity. Here, we briefly explore several implications that dry rock model results have for four common types of reservoir-derived volcanic features.

Summit eruptions and edifice growth. Dry rock model data indicate that many paths will lead to the creation of edifices fed by central eruptions from a near-surface magma reservoir, consistent with abundant observations of such features on the terrestrial planets (e.g. Head & Wilson 1992; Wilson & Head 1994). To illustrate the interplay between magma reservoir rupture and edifice growth, consider a spherical reservoir with $R/DtC = 0.45$. Emplaced beneath a surface with negligible topography, the overpressure required to induce rupture will be roughly twice the lithostatic load at the crest (Fig. 2). Shallow reservoirs will, thus, fail more readily than those located at greater depths and, upon rupture, circumferential intrusions initiated at α of approximately 60° will result (Fig. 3), directing magma towards shallower depths. Dykes that breach the surface will begin to emplace lavas and other deposits, perhaps initially in a distributed fashion given the geometry of the intrusions. Whether widespread layers are emplaced – which, in effect, means that the reservoir crest lies at progressively greater depth – or an edifice begins to grow, the surface load will begin to rotate the point of failure towards the reservoir crest. Once vertical dyke injection from the crest is established, magma can be transported with maximum efficiency towards the surface, and growing conical edifices with summit eruptions become the expected volcanic norm unless tectonic stresses or other factors, such as basal slip, modify the edifice stress regime. The edifice size required to produce noticeable rupture point rotation depends on the reservoir radius and the edifice flank slope (i.e. shield- or stratocone-like) but, for reservoirs with R ranging from 0.2 to 4 km, typical edifice radii of the order of 5 km prove sufficient (cf. fig. 4 of Hurwitz *et al.* 2009). As an edifice grows in size, for a time the magma system stabilizes: failure locked at the reservoir crest will feed material efficiently towards the edifice summit and, simultaneously, the overpressure required for failure decreases (Fig. 2b), which means that rupture and upwards propagation of magma via vertical dykes will occur more readily. As the edifice size increases significantly, the effective depth of the reservoir increases as well, a feedback mechanism that stabilizes the system by elevating the pressure needed for rupture (perhaps allowing the reservoir to increase in size). Eventually, however, if the magma system remains active, the growing load from the volcano can begin to induce significant flexure. The magnitude of the flexural response and the impact on reservoir rupture depends on the elastic thickness of the lithosphere and the reservoir depth due to the hourglass-like pattern of the flexural stresses. Generally speaking, however, an edifice with a radius above several tens of kilometres can induce sufficient flexure to terminate rupture at the crest of a typical kilometre-scale reservoir, aborting direct vertical magma ascent, unless elastic thicknesses are very large, the lithosphere is unusually weak and/or the reservoir depth is very great (Murphy *et al.* 2012). Depending on the specific volcanic configuration, lateral re-direction of magma by flexural stresses can terminate edifice growth and limit edifice size, or it may redirect magma to the surface via flank eruptions that act to modify the edifice morphology (McGovern *et al.* 2013).

Circumferential intrusions. Although observed less often in modern settings, circumferential intrusions are a common element of older eroded volcanic systems (Chadwick *et al.* 2011). It has also been proposed that such features could be responsible for circumferential fracture systems observed on Venus (common) and Mars (rare), but proving this connection has been difficult as circumferential fractures can form via a variety of volcanic and tectonic mechanisms (Ernst *et al.* 2001). Even the clearest evidence of magma involvement – lava flows emerging occasionally from individual structures within sets of circumferential fractures – are problematic, for this could imply either that circumferential dykes ascending to shallow depth generate the fractures (e.g. Mastin & Pollard 1988) or that other dykes encountering a pre-existing tectonic fracture set with a circumferential geometry simply utilize it to reach the surface more easily.

Dry rock model results predict that shallow- to steeply-dipping circumferential intrusions can form in response to inflation of spherical or oblate reservoirs, predominantly at shallow scaled depths (Grosfils 2007; Hurwitz *et al.* 2009); for a spherical reservoir, dips steeper than 55° are expected,

while oblate reservoirs tend to intrude dykes only at shallower dips (Fig. 3). Edifice loading in the absence of flexure will normally increase the dip expected at a given scaled depth (the exception occurs for more oblate reservoirs, where little change in dip occurs: Hurwitz *et al.* 2009). Older systems exhibiting circumferential intrusions (e.g. Clough *et al.* 1909) may, thus, record the initial or pre-edifice stages of volcanism at a given shallow magmatic centre, only exposed by deep erosion, because resulting edifice growth tends to shut down circumferential intrusion (see the subsection on 'Summit eruptions and edifice growth') while burying older intrusion signatures with younger lavas. Significant downwards flexure will make it exceedingly difficult for circumferential intrusions to feed dykes toward the surface (Galgana *et al.* 2011), but bulk stress states induced by surface loading can promote lateral propagation from the reservoir and then circumferential dyke ascent at greater distances from the symmetry axis, a mechanism that may help explain the growth of domical and annular edifices (McGovern *et al.* 2013).

Lateral radial dyke swarm formation. An unexpected result from dry rock models is that laterally propagating radial dykes, commonly observed on Earth, Venus and Mars, are difficult to explain as a direct product of magma reservoir inflation and rupture. Previous analyses using 'overpressure only' formulations have implied that lateral dyke initiation is straightforward, but the models do not examine the wall-parallel stresses σ_t and σ_θ independently, and generally assume that rupture at the mid-depth leads directly to lateral dyke injection (e.g. Parfitt *et al.* 1993). In fact, duplication of these model conditions reveals that rupture near the mid-section occurs in the σ_t orientation, and will emplace lateral sills (Grosfils 2007). Similarly, dry rock models predict patterns of failure that produce vertical radial dyke ascent from the crest, lateral sill injection or the emplacement of inclined circumferential intrusions. Only in three very specific circumstances have conditions conducive to lateral radial dyke propagation been identified.

First, growth of an edifice at the surface can create a stress trap capable of redirecting magma from vertical ascent to lateral propagation at shallow depth, in essence right along the base of the edifice (Hurwitz *et al.* 2009). The lateral extent of this stress trap is limited by the edifice radius, and will not permit lateral dyke injection to continue beyond this distance unless such propagation is enabled by other factors (e.g. Parfitt & Head 1993; Pinel & Jaupart 2004). Tests striving to match data from Summer Coon (Poland *et al.* 2008) reveal that the model predictions closely simulate measured dyke depth, extent and thickness variations (Hurwitz *et al.* 2009), indicating that this mechanism can explain typical lateral dyke injection patterns often observed at composite volcanoes. Second, while Hurwitz *et al.* (2009) restrict their analysis to sub-edifice reservoirs, subsequent efforts examining rupture of reservoirs that lie partially within an edifice have shown that volcanologically plausible evolution of a mildly oblate reservoir's aspect ratio can initiate both circumferential and lateral dyke injection within an edifice (Fig. 7). Tests by Chestler & Grosfils (2013) striving to match complex intrusion patterns reported for the Galapagos (e.g. Chadwick *et al.* 2011; Bagnardi *et al.* 2013) do so using a reservoir configuration consistent with existing size and depth constraints but, again, the lateral extent of the radial dykes will be limited. Third, at a much larger scale, lateral dykes can occur when broad flexural upwarping, generated by a zone of melt at the base of the lithosphere that creates conditions conducive to

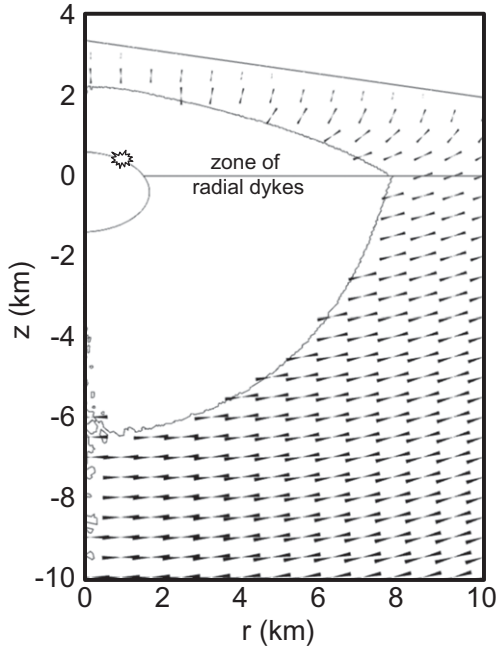

Fig. 7. Model depicting radial dyke initiation within a conical edifice ($V_h = 3.4$ km, $V_r = 23.7$ km; akin to a Galapagos-sized volcano). Reservoir is centred at $z = -0.4$ km, with $R_b = 1$ km and $R_a = 1.7$ km. Short linear symbols denote alignment of the minimum compressive stress, and are perpendicular to the page where missing in the zone surrounding the reservoir. Orientation of the fracture formed when initial failure occurs (at the star, $z = 0.4$ km) will inject a radial dyke laterally into the edifice within a zone where the stress state strongly favours continued radial dyke stability.

surface eruption, is integrated with downwarping introduced as the resulting surface load grows (Galgana *et al.* 2013). For an edifice the size of a typical large Venusian volcano, this combination produces a stress trap at the base of the edifice similar to that identified by Hurwitz *et al.* (2009). It differs, however, in that the basal uplift affects the stress state across a much broader area, creating conditions in which lateral dykes are more likely to propagate across distances akin to those observed in many giant radial systems (Grosfils & Head 1994; Ernst *et al.* 1995).

While the results summarized above are certainly encouraging, all three mechanisms require the presence of an edifice at the surface. In many instances this condition is met, but observations from Venus indicate that, of the 118 giant radiating dyke swarms identified in an initial global survey, roughly half do not exhibit evidence of the necessary elevated (domical or edifice-like) central topography (Grosfils & Head 1994). While constraints upon the topography of similar systems on Earth are limited (e.g. Ernst *et al.* 1995), the Venusian data indicate that roughly half of the giant radial dyke swarms identified cannot be explained using the three mechanisms described above. Further research in this area is clearly required.

Caldera formation. As discussed above, preliminary results demonstrate that the conditions necessary for initiating ring faults develop more readily than previously believed, and that special circumstances such as basal uplift or regional tension are not required. When conditions are primed for throughgoing ring faults to form as a result of magma reservoir inflation, the expected geometry – matching proposed criteria (Gudmundsson 1998; Folch & Marti 2004) – is a steep, inwards-dipping normal fault anchored in a zone of shear failure at depth (Fig. 6). The ring fault formation predicted by dry rock models differs from proposed criteria in that rupture initiates at the reservoir wall, not at the surface; this matches data from caldera formation events monitored in the field (e.g. Geshi *et al.* 2002).

From limited analyses to date there are several implications for the mechanics of caldera formation in a planetary context. First, caldera formation, while almost certainly aided by factors such as basal uplift and regional extension (Gudmundsson 2007) or edifice loading (Pinel & Jaupart 2005), does not require these external drivers. Calderas should occur wherever inflation of a suitable reservoir geometry primes the host rock for ring faulting, and the presence of a caldera does not imply that precursory tectonic activity of a specific kind occurred at the site. Second, given the dependence of Mohr–Coulomb shear failure on normal stress magnitude and, hence, gravitational loading, an inflating reservoir at identical depths on Earth and Mars is expected to generate ring faults and form calderas more readily on Mars. Third, however, because reservoirs are likely to form at proportionately greater depths on Mars than they do on Earth (e.g. Wilson & Head 1994), which changes the aspect ratio of the roof rock above a reservoir, this should adversely affect the likelihood that a ring fault on Mars will reach the surface (e.g. Roche *et al.* 2000). Thus, unless they form above unusually shallow reservoirs, calderas are expected to be rarer on Mars than on rocky planets with higher gravity (i.e. Earth and Venus). To first order, this is consistent with what is observed (e.g. Radebaugh *et al.* 2001; Sanchez & Shcherbakov 2012), but some caution is warranted as caldera detection capabilities and preservation likelihood are not equivalent on these three bodies, and further work is required to test the validity of the proposed link between reservoir mechanics and caldera observations on the terrestrial planets.

Applicability and limitations of elastic models

Field and geophysical data demonstrate that subsurface magma reservoirs are long-lived mechanically and thermally complex systems (e.g. de Silva *et al.* 2006), and it is reasonable to expect that elastic continuum numerical models can provide only limited insight into their evolution and the volcanic consequences. Complementing physical–chemical model assessments that explore the role played by magma evolution during an eruption (cf. Karlstrom *et al.* 2012; Segall 2013), their primary use when assessing inflation has been to predict the conditions that prime a system for rupture, and to then project the expected outcome based on the assumption that the host rock stress state dictates subsequent rupture evolution and/or intrusion path. Continuum elastic models are generally unable, however, to track critical factors that probably play a key role in such activity, such as time-dependent fatigue (induced by repeated inflation–deflation cycles, for instance: e.g. Kendrick *et al.* 2013) or the dynamic stress changes associated with intrusion propagation or shear crack displacement (e.g. Meriaux & Lister 2002; Shuler *et al.* 2013). The attraction of elastic numerical models in spite of these concerns is that: (a) they can describe bulk system behaviour adequately, particularly for a process such as inflation, which responds rapidly to changes in the system; (b) they are easy to implement and require minimal time or computing power to run; and (c) the simplicity of their components means that they can be calibrated carefully using analytical

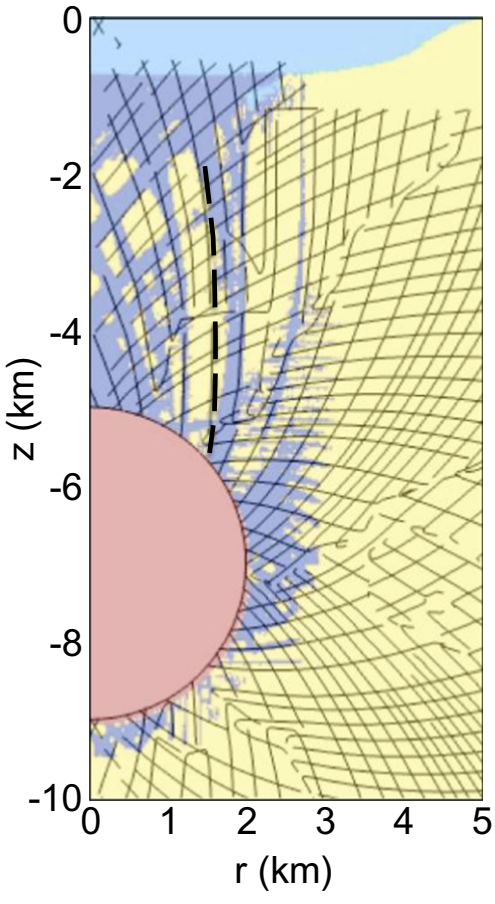

Fig. 8. Mohr–Coulomb failure planes predicted for a spherical reservoir ($R = 2$ km, $DtC = 7$ km, $\Delta P = 130$ MPa) within a dry elastic host rock, superimposed on elasto-plastic strain results reported by Gerbault *et al.* (2012) for the same conditions. Dark blue regions denote areas of plastic shear failure, while the light blue region denotes the area of tensile failure; yellow indicates intact rock. There is excellent agreement between the shear failure orientations predicted by the two approaches. Using the method illustrated in Figure 6, the only plausible location for ring fault development in the dry elastic host rock model results is shown by a heavy dashed line. While offset slightly from the main ring fault-like zone of shear in the elasto-plastic model, the two results agree quite well, and the elastic model yields similar first-order insight into expected ring fault nucleation and geometry.

solutions. Elastic numerical model solutions, in turn, provide an important framework for calibrating advanced models that incorporate factors such as temperature-dependent rheology and plastic strain (e.g. Jellinek & DePaolo 2003; Trasatti *et al.* 2005; Del Negro *et al.* 2009).

Given their obvious limitations and simplicity, how useful are the results from elastic models, and how well do they perform when compared with more advanced solutions? Perhaps surprisingly, the answer is that they do remarkably well for a wide array of volcanologically plausible configurations. For instance, Gregg *et al.* (2012) used a temperature-dependent viscoelastic model formulation to study the overpressure needed to induce throughgoing rupture, and concluded that the solutions did not diverge noticeably from the outcomes of purely elastic dry rock solutions (e.g. Grosfils 2007) until reservoirs reach volumes of the order of 10^2–10^3 km^3 (i.e. comparable to volumes inferred for Taupo caldera, New Zealand: Ellis *et al.* 2007) with small roof aspect ratios ($R_a > 3D$). Similarly, the Mohr–Coulomb failure plane orientations used to assess potential for ring fault development in a dry rock elastic formulation compare well with detailed plane strain elasto-plastic models (Gerbault *et al.* 2012) that track time-dependent shear failure and fracture development above both inflating and deflating magma reservoirs (Fig. 8). In spite of this agreement, elasto-plastic model results represent a significant advance in that they predict which planes are more likely to serve as sites for throughgoing ring fault nucleation and growth. It is also worth noting, however, that analysis of spherical geometries requires computations that individually can take weeks–months to run, a significant limitation considering an elastic model formulation such as ours can predict a similar outcome (Fig. 8) using computations that require only minutes to complete.

Conclusions

Numerical elastic continuum models of magma reservoir inflation can provide insights applicable to a surprisingly diverse array of volcanic conditions. When integrated with field, laboratory and remote-sensing data gathered on Earth and from other planets, such models have already provided important new insight into many common reservoir-related processes such as edifice construction, caldera formation and radial dyke injection. In part, this is because many factors of volcanological importance can be considered within an elastic model framework. Complementing uniform homogeneous simulations, for example, models can easily introduce magma and host rock density variations, or explore the impacts of mechanical layering, edifice loading and flexure. Furthermore, elastic model components and predictions are largely insensitive to, or can readily incorporate and assess, material and parameter variations that characterize

different planetary environments. Finally, when compared with models incorporating more advanced behaviour (e.g. Holohan *et al.* 2007; Gerbault *et al.* 2012) that can require weeks or months to run, elastic models are simple to design and test, take minutes or hours to execute, yet often produce results that are directly comparable to those obtained using more complex approaches. As a result, although one must remain cognizant of their limitations, elastic models of magma reservoir inflation and rupture have become a key tool for understanding planetary volcanism.

In spite of recent advances, however, there are three areas where existing model results indicate that additional research will be of particular benefit for addressing outstanding questions and advancing modelling capabilities. The first area pertains to the role of pore pressure variations within the host rock surrounding a magma reservoir. Models that assume dry rock conditions develop a baseline framework for understanding magma reservoir inflation and rupture on this basis. More traditional 'overpressure only' formulations that assume lithostatic pore pressure have been widely used for decades, however, and they make markedly different predictions when assessing the rupture overpressure, location and orientation, as well as the surface uplift magnitude that can occur prior to tensile failure and intrusion. Given these differences, it has become critical to obtain better insight than volcanologists have at present into: (a) the pore pressure conditions that normally occur within host rock surrounding an active magma reservoir; and (b) the range of plausible pore pressures, and what controls their spatial and temporal variability. As noted by Gerbault *et al.* (2012), major variations in pore pressure within the host rock adjacent to a magma reservoir could lead to rupture without any changes to an existing magma overpressure.

The second area we identify for additional research focuses on the need to address specific recognized gaps in existing knowledge, which become apparent when a given type of volcanic feature cannot be reproduced as expected; several key examples are identified in the subsections on 'Uniform and layered half-space models', 'Models with edifice loading' and 'Implications for reservoir-related planetary volcanism'. For example, while we have reported several different ways to initiate laterally propagating radial dykes (see the subsection 'Lateral radial dyke swarm formation'), all require the presence of an edifice or comparable load at the surface. However, many radial dyke swarms clearly formed without this condition in place (Grosfils & Head 1994), which begs the question of what is missing from current model formulations – dry rock and 'overpressure only' alike. Addressing core questions like this example, although seemingly somewhat narrow in focus, remains exceedingly important. Inability to reproduce common volcanic situations probably indicates that fundamental framing of numerical magma reservoir inflation simulations by the volcanological community may be neglecting some key factor (e.g. magmas are treated as fluids, yet magmas convect and, thus, couple shear stress to the reservoir wall). Returning to the dyke swarm example, identifying how to produce laterally propagating radial dykes across a wider array of conditions may help refine the fundamental framing of magma reservoir inflation models in ways that inform elastic and more complex models alike.

Finally, in spite of the benefits realized to date using elastic models, there are obvious motivations for improving more complex model formulations (e.g. discrete element, elasto-plastic and viscoelastic). Advances in these directions require moving beyond two-dimensional (2D) plane stress–strain models that treat reservoirs as a slice through a horizontal cylinder, however, and beyond axisymmetrical models like those reported on here that permit rapid parameterized analyses of ellipsoidal and similar geometries. Indeed, the benefits of 3D models of individual volcanoes that incorporate spatially variable material properties, irregular topography and regional tectonic stresses are beginning to be exploited (e.g. Bonaccorso *et al.* 2005). Ultimately, once calibrated against carefully framed and understood elastic model results, continued development of advanced 3D model formulations shows exceptional promise as a means of improving geologists' insight into volcanic phenomena on Earth and other rocky bodies in the solar system.

We are grateful for many thought-provoking conversations about magma reservoir mechanics over the years with J. Head, A. Newman, E. Parfitt, M. Parmentier, A. Rubin, S. de Silva and L. Wilson. We also thank two anonymous reviewers for suggestions that enhanced the manuscript. This work was supported in part by NASA grants NAG5-9618, NAG5-10498, NNG05GJ92G and NNX08AL77G, with additional student involvement supported by the Summer Undergraduate Research Program at, and a Mellon Post-Baccalaureate Fellowship from, Pomona College.

References

Acocella, V. 2008. Structural development of calderas: a synthesis from analogue experiments. *In*: Gottsman, J. & Marti, J. (eds) *Caldera Volcanism: Analysis, Modelling and Response*. *Developments in Volcanology*, **10**, 285–311.

Anderson, E. M. 1936. Dynamics of the formation of cone-sheets, ring-dykes, and cauldron-subsidences. *Proceedings of the Royal Society of Edinburgh*, **56**, 128–157.

Bachmann, O. & Bergantz, G. W. 2004. On the origin of crystal-poor rhyolites: extracted from batholithic crystal mushes. *Journal of Petrology*, **45**, 1565–1582.

Baker, S. & Amelung, F. 2012. Top-down inflation and deflation at the summit of Kilauea volcano, Hawai'i observed with InSAR. *Journal of Geophysical Research*, **117**, B12406, 1–14.

Bagnardi, M., Amelung, F & Poland, M. P. 2013. A new model for the growth of basaltic shields based on deformation of Fernandina volcano, Galapagos Islands. *Earth and Planetary Science Letters*, **377–378**, 358–366, http://dx.doi.org/10.1016/j.epsl.2013.07.016

Bartel, B. A., Hamburger, M. W., Meertens, C. M., Lowry, A. R. & Corpuz, E. 2003. Dynamics of active magmatic and hydrothermal systems at Taal Volcano, Philippines, from continuous GPS measurements. *Journal of Geophysical Research*, **108**, 2475, http://dx.doi.org/10.1029/2002JB002194

Battaglia, M., Segall, P., Murray, J., Cervelli, P. & Langbein, J. 2003. The mechanics of unrest at Long Valley caldera, California: 1. Modeling the geometry of the source using GPS leveling and two-color EDM data. *Journal of Volcanology and Geothermal Research*, **127**, 195–217.

Berrino, G., Corrado, G., Luongo, G. & Toro, B. 1984. Ground deformation and gravity changes accompanying the 1982 Pozzuoli uplift. *Bulletin of Volcanology*, **47**, 187–200.

Blake, S. 1981. Volcanism and dynamics of open magma chambers. *Nature*, **289**, 783–785.

Bonaccorso, A. & Davis, P. M. 1999. Models of ground deformation from vertical volcanic conduits with application to eruptions of Mount St. Helens and Mount Etna. *Journal of Geophysical Research*, **104**, 10,531–10,542.

Bonaccorso, A., Cianetti, S., Giunchi, C., Trasatti, E., Bonafede, M. & Boschi, E. 2005. Analytical and 3-D numerical modeling of Mt. Etna (Italy) volcano inflation. *Geophysical Journal International*, **163**, 852–862.

Brace, W. F. 1980. Permeability of crystalline and argillaceous rocks. *International Journal of Rock Mechanics and Mining Sciences and Geomechanics Abstracts*, **17**, 241–251.

Burgisser, A. & Bergantz, G. W. 2011. A rapid mechanism to remobilize and homogenize highly crystalline magma bodies. *Nature*, **471**, 212–215.

Cashman, K. V. & Sparks, R. S. J. 2013. How volcanoes work: a 25 year perspective. *Geological Society of America Bulletin*, **125**, 664–690.

Cervelli, P., Murray, M., Segall, P., Aoki, Y. & Kato, T. 2001. Estimating source parameters from deformation data, with an application to the March 1997 earthquake swarm off the Izu Peninsula, Japan. *Journal of Geophysical Research*, **106**, 11,217–11,237.

Chadwick, W. W. & Dieterich, J. H. 1995. Mechanical modeling of circumferential and radial dike intrusion on Galapagos volcanoes. *Journal of Volcanology and Geothermal Research*, **66**, 37–52.

Chadwick, W. W., Jonsson, S. *et al.* 2011. The May 2005 eruption of Fernandina Volcano, Galapagos; the first circumferential dike intrusion observed by GPS and InSAR. *Bulletin of Volcanology*, **73**, 679–697.

Chaussard, E. & Amelung, F. 2012. Precursory inflation of shallow magma reservoirs at west Sundra volcanoes detected by InSAR. *Geophysical Research Letters*, **39**, L21311, http://dx.doi.org/10.1029/2012GL053817

Chestler, S. R & Grosfils, E. B. 2013. Using numerical modeling to explore the origin of intrusion patterns on Fernandina volcano, Galapagos islands, Ecuador. *Geophysical Research Letters*, **40**, 4565–4569, http://dx.doi.org/10.1002/grl.50833

Christensen, J. N. & DePaolo, D. J. 1993. Time scales of large volume silicic magma systems: Sr isotope systematics of phenocrysts and glass from the Bishop Tuff, Long Valley, California. *Contributions to Mineralogy and Petrology*, **113**, 100–114.

Clough, C. T., Maufe, H. B. & Bailey, E. B. 1909. The cauldron-subsidence of Glen Coe, and the associated igneous phenomena. *Quarterly Journal of the Geological Society, London*, **65**, 611–678.

Currenti, G., Bonaccorso, A., Del Negro, C., Scandura, D. & Boschi, E. 2010. Elasto-plastic modeling of volcano ground deformation. *Earth and Planetary Science Letters*, **296**, 311–318.

Davis, P. M. 1986. Surface deformation due to inflation of an arbitrarily oriented triaxial ellipsoidal cavity in an elastic half-space, with reference to Kilauea volcano, Hawaii. *Journal of Geophysical Research*, **91**, 7429–7438.

de Silva, S. L., Zandt, G., Trumbull, R., Viramonte, J. G., Salas, G. & Jimenez, N. 2006. Large ignimbrite eruptions and volcano-tectonic depressions in the Central Andes: a thermomechanical perspective. *In*: Troise, C., De Natale, G. & Kilburn, C. R. J. (eds) *Mechanisms of Activity and Unrest at Large Calderas*. Geological Society, London, Special Publications, **269**, 47–63.

Del Negro, C., Currenti, G. & Scandura, D. 2009. Temperature-dependent viscoelastic modeling of ground deformation: application to Etna volcano during the 1993–1997 inflation period. *Physics of the Earth and Planetary Interiors*, **172**, 299–309.

Dieterich, J. H. & Decker, R. W. 1975. Finite-element modeling of surface deformation associated with volcanism. *Journal of Geophysical Research*, **80**, 4094–4102.

Druitt, T. H., Costa, F., Deloule, E., Dungan, M. & Scaillet, B. 2012. Decadal to monthly timescales of magma transfer and reservoir growth at a caldera volcano. *Nature*, **482**, 77–80.

Dzurisin, D. 2003. A comprehensive approach to monitoring volcano deformation as a window on the eruption cycle. *Reviews of Geophysics*, **41**, 1–5, http://dx.doi.org/10.1029/2001RG000107

Ellis, S. M., Wilson, C. J. N., Bannister, S., Bibby, H. M., Heise, W., Wallace, L. & Patterson, N. 2007. A future magma inflation event under the rhyolitic Taupo volcano, New Zealand: numerical models based on constraints from geochemical, geological and geophysical data. *Journal of Volcanology and Geothermal Research*, **168**, 1–27.

Engelder, T. & Leftwich, J. T. 1997. A pore-pressure limit in overpressured south Texas oil and gas fields. *In*: Surdam, R. C. (ed.) *Seals, Traps, and the*

Petroleum System. American Association of Petroleum Geologists, Memoirs, **67**, 255–267.

ERNST, R. E., HEAD, J. W., PARFITT, E., GROSFILS, E. B. & WILSON, L. 1995. Giant radiating dyke swarms on Earth and Venus. *Earth Science Reviews*, **39**, 1–58.

ERNST, R. E., GROSFILS, E. B. & MEGE, D. 2001. Giant dike swarms: Earth, Venus and Mars. *Annual Review of Earth and Planetary Sciences*, **29**, 489–534.

FIALKO, Y., KHAZAN, Y. & SIMONS, M. 2001. Deformation due to a pressurized horizontal circular crack in an elastic half-space, with applications to volcano geodesy. *Geophysical Journal International*, **146**, 181–190.

FOLCH, A. & MARTI, J. 2004. Geometrical and mechanical constraints on the formation of ring-fault calderas. *Earth and Planetary Science Letters*, **221**, 215–225.

GALGANA, G. A., MCGOVERN, P. J. & GROSFILS, E. B. 2011. Evolution of large Venusian volcanoes: insights from coupled models of lithospheric flexure and magma reservoir pressurization. *Journal of Geophysical Research*, **116**, E03009, http://dx.doi.org/10.1029/2010JE003654

GALGANA, G. A., GROSFILS, E. B. & MCGOVERN, P. J. 2013. Radial dike formation on Venus: insights from models of uplift, flexure and magmatism. *Icarus*, **225**, 538–547.

GERBAULT, M. 2012. Pressure conditions for shear and tensile failure around a circular magma chamber: insight from elasto-plastic modeling. *In*: HEALY, D., BUTLER, R. W. H., SHIPTON, Z. & SIBSON, R. H. (eds) *Faulting, Fracturing and Igneous Intrusion in the Earth's Crust*. Geological Society, London, Special Publications, **367**, 111–130.

GERBAULT, M., CAPPA, F. & HASSANI, R. 2012. Elasto-plastic and hydromechanical models of failure around an infinitely long magma chamber. *Geochemistry, Geophysics, Geosystems*, **13**, Q03009, http://dx.doi.org/10.1029/2011GC003917

GERTISSER, R., SELF, S., THOMAS, L. E., HANDLEY, H. K., VAN CALSTEREN, P. & WOLFF, J. A. 2012. Processes and timescales of magma genesis and differentiation leading to the great Tambora eruption in 1815. *Journal of Petrology*, **53**, 271–297.

GESHI, N., SHIMANO, T., CHIBA, T. & NAKADA, S. 2002. Caldera collapse during the 2000 eruption of Miyakejima Volcano, Japan. *Bulletin of Volcanology*, **64**, 55–68.

GEYER, A. & GOTTSMANN, J. 2010. The influence of mechanical stiffness on caldera deformation and implications for the 1971–1984 Rabaul uplift (Papua New Guinea). *Tectonophysics*, **483**, 399–412.

GEYER, A. & BINDEMAN, I. 2011. Glacial influence on caldera-forming eruptions. *Journal of Volcanology and Geothermal Research*, **202**, 127–142.

GOTTSMANN, J., FOLCH, A. & RYMER, H. 2006. Unrest at Campi Flegrei: a contribution to the magmatic v. hydrothermal debate from inverse and finite element modeling. *Journal of Geophysical Research*, **111**, B07203, http://dx.doi.org/10.1029/2005JB003745

GREGG, P. M., DE SILVA, S. L., GROSFILS, E. B. & PARMIGIANI, J. P. 2012. Catastrophic caldera-forming eruptions: thermomechanics and implications for eruption triggering and maximum caldera dimensions on Earth. *Journal of Volcanology and Geothermal Research*, **241–242**, 1–12.

GROSFILS, E. B. 2007. Magma reservoir failure on the terrestrial planets: assessing the importance of gravitational loading in simple elastic models. *Journal of Volcanology and Geothermal Research*, **166**, 47–75.

GROSFILS, E. B. 2011. New mechanical insights into ring fault initiation and caldera formation on terrestrial planets. *In*: *42nd Lunar and Planetary Science Conference, held 7–11 March 2011 at The Woodlands, Texas*. Lunar and Planetary Institute, Houston, TX, Abstract 1170.

GROSFILS, E. B. & HEAD, J. W. 1994. The global distribution of giant radiating dike swarms on Venus: implications for the global stress state. *Geophysical Research Letters*, **21**, 701–704.

GROSSE, P., VAN WYCK DE VRIES, B., PETRINOVIC, I. A., EUILLADES, P. A. & ALVARADO, G. E. 2009. Morphometry and evolution of arc volcanoes. *Geology*, **37**, 651–654.

GUALDA, G. A. R., PAMUKCU, A. S., GHIORSO, M. S., ANDERSON, A. T., SUTTON, S. R. & RIVERS, M. L. 2012. Timescales of quartz crystallization and the longevity of the Bishop giant magma body. *PLoS ONE*, **7**, 1–12.

GUDMUNDSSON, A. 1988. Effect of tensile stress concentration around magma chambers on intrusion and extrusion frequencies. *Journal of Volcanology and Geothermal Research*, **35**, 179–194.

GUDMUNDSSON, A. 1998. Formation and development of normal-fault calderas and the initiation of large explosive eruptions. *Bulletin of Volcanology*, **60**, 160–170.

GUDMUNDSSON, A. 1990. Emplacement of dikes, sills and crustal magma chambers at divergent plate boundaries. *Tectonophysics*, **176**, 257–275.

GUDMUNDSSON, A. 2006. How local stresses control magma-chamber ruptures, dyke injections, and eruptions in composite volcanoes. *Earth Science Reviews*, **79**, 1–31.

GUDMUNDSSON, A. 2007. Conceptual and numerical models of ring-fault formation. *Journal of Volcanology and Geothermal Research*, **164**, 142–160.

GUDMUNDSSON, A. 2012. Magma chambers: formation, local stresses, excess pressures, and compartments. *Journal of Volcanology and Geothermal Research*, **237–238**, 19–41.

HEAD, J. W. & WILSON, L. 1992. Magma reservoirs and neutral buoyancy zones on Venus: implications for the formation and evolution of volcanic landforms. *Journal of Geophysical Research*, **97**, 3877–3903.

HILDRETH, W. 1981. Gradients in silicic magma chambers: implications for lithospheric magmatism. *Journal of Geophysical Research*, **86**, 10,153–10,192.

HOBBS, T. 2011. *Stress Induced Seismic Anisotropy Around Magma Chambers*. PhD thesis, University of Bristol, UK.

HOLOHAN, E. P., SCHOPFER, M. P. J. & WALSH, J. J. 2007. Mechanical and geometric controls on the structural evolution of pit crater and caldera subsidence. *Journal of Geophysical Research*, **116**, B07202, http://dx.doi.org/10.1029/2010JB008032

HUBBERT, M. K. & RUBEY, W. W. 1959. Role of fluid pressure in mechanics of overthrust faulting. *Geological Society of America Bulletin*, **70**, 115–166.

HUBER, C., BACHMANN, O. & DUFEK, J. 2012. Crystal-poor v. crystal-rich ignimbrites: a competition between stirring and reactivation. *Geology*, **40**, 115–118.

HURWITZ, D. M., LONG, S. M. & GROSFILS, E. B. 2009. The characteristics of magma reservoir failure beneath a volcanic edifice. *Journal of Volcanology and Geothermal Research*, **188**, 379–394.

JAEGER, J. C. & COOK, N. G. W. 1979. *Fundamentals of Rock Mechanics*. Chapman & Hall, New York.

JEFFREY, G. B. 1921. Plane stress and plane strain in bipolar coordinates. *Philosophical Transactions of the Royal Society of London, Series A*, **221**, 265–293.

JELLINEK, A. M. & DEPAOLO, D. J. 2003. A model for the origin of large silicic magma chambers: precursors of caldera-forming eruptions. *Bulletin of Volcanology*, **65**, 363–381.

KARLSTROM, L., RUDOLPH, M. L. & MANGA, M. 2012. Caldera size modulated by the yield stress within a crystal-rich magma reservoir. *Nature Geoscience*, **5**, 402–405.

KENDRICK, J. E., SMITH, R., SAMMONDS, P., MEREDITH, P. G., DAINTY, M. & PALLISTER, J. S. 2013. The influence of thermal and cyclic stressing on the strength of rocks from Mount St. Helens, Washington. *Bulletin of Volcanology*, **75**, 752, http://dx.doi.org/10.1007/s00445–013–0728-z

KENNEDY, B., STIX, J., VALLANCE, J. W., LAVALLEE, Y. & LONGPRE, M.-A. 2004. Controls on caldera structure: results from analogue sandbox modeling. *Geological Society of America Bulletin*, **116**, 515–524.

KOENIG, E. & POLLARD, D. D. 1998. Mapping and modeling of radial fracture patterns on Venus. *Journal of Geophysical Research*, **103**, 15183–15202.

KOHLSTEDT, D. L. & MACKWELL, S. J. 2010. Strength and deformation of planetary lithospheres. *In*: WATTERS, T. R. & SCHULTZ, R. A. (eds) *Planetary Tectonics*. Cambridge University Press, New York.

LETOURNEUR, L., PELTIER, A., STAUDACHER, T. & GUDMUNDSSON, A. 2008. The effects of rock heterogeneities on dyke paths and asymmetric ground deformation: the example of Piton de la Fournaise (Reunion Island). *Journal of Volcanology and Geothermal Research*, **173**, 289–302.

LOCKNER, D. & BYERLEE, J. D. 1977. Hydrofracture in Weber sandstone at high confining pressure and differential stress. *Journal of Geophysical Research*, **82**, 2018–2026.

LONG, S. M. & GROSFILS, E. B. 2009. Modeling the effect of layered volcanic material on magma reservoir failure and associated deformation, with application to Long Valley caldera, California. *Journal of Volcanology and Geothermal Research*, **186**, 349–360.

MACCAFERRI, F., BONAFEDE, M. & RIVALTA, E. 2011. A quantitative study of the mechanisms governing dike propagation, dike arrest and sill formation. *Journal of Volcanology and Geothermal Research*, **208**, 39–50.

MANCONI, A., WALTER, T. R. & AMELUNG, F. 2007. Effects of mechanical layering on volcano deformation. *Geophysical Journal International*, **170**, 952–958.

MANCONI, A., WALTER, T., MANZO, M., ZENI, G., TIZZANI, P., SANSOSTI, E. & LANARI, R. 2010. On the effects of 3-D mechanical heterogeneities at Campi Flegrei caldera, southern Italy. *Journal of Geophysical Research*, **115**, B08405, http://dx.doi.org/10.1029/2009JB007099

MARTI, J., GEYER, A., FOLCH, A. & GOTTSMAN, J. 2008. A review on collapse caldera modelling. *In*: GOTTSMAN, J. & MARTI, J. (eds) *Caldera Volcanism: Analysis, Modelling and Response*. *Developments in Volcanology*, **10**, 233–283.

MASTERLARK, T. 2007. Magma intrusion and deformation predictions: sensitivities to the Mogi assumptions. *Journal of Geophysical Research*, **112**, B06419, http://dx.doi.org/10.1029/2006JB004860

MASTIN, L. G. & POLLARD, D. D. 1988. Surface deformation and shallow dike intrusion processes at Inyo craters, Long Valley, CA. *Journal of Geophysical Research*, **93**, 13,221–13,235.

MATTHEWS, N. E., HUBER, C., PYLE, D. M. & SMITH, V. C. 2012. Timescales of magma recharge and reactivation of large silicic systems from Ti diffusion in quartz. *Journal of Petrology*, **53**, 1385–1416.

MCGARR, A. 1988. On the state of lithospheric stress in the absence of applied tectonic forces. *Journal of Geophysical Research*, **93**, 13,609–13,617.

MCGOVERN, P. J. & SOLOMON, S. C. 1993. State of stress, faulting, and eruption characteristics of large volcanoes on Mars. *Journal of Geophysical Research*, **98**, 23,553–23,579.

MCGOVERN, P. J., GROSFILS, E. B. *ET AL.* 2013. Lithospheric flexure: the key to the structural evolution of large volcanic edifices on the terrestrial planets. *In*: MASSIRONI, M., BYRNE, P., HIESINGER, H. & PLATZ, T. (eds) *Volcanism and Tectonism Across the Solar System*. Geological Society, London, Special Publications, **401**. First published online Month XX, 2013, http://dx.doi.org/10.1144/SP394.XX

MCLEOD, P. & TAIT, S. 1999. The growth of dykes from magma chambers. *Journal of Volcanology and Geothermal Research*, **92**, 231–245.

MCTIGUE, D. F. 1987. Elastic stress and deformation near a finite spherical magma body: resolution of a point source paradox. *Journal of Geophysical Research*, **92**, 12,931–12,940.

MERIAUX, C. & LISTER, J. R. 2002. Calculation of dike trajectories from volcanic centers. *Journal of Geophysical Research*, **107**, ETG 10-1–ETG 10-10, http://dx.doi.org/10.1029/2001JB000436

MOGI, K. 1958. Relationships between the eruptions of various volcanoes and the deformation of the ground surfaces around them. *Bulletin of the Earthquake Research Institute, University of Tokyo*, **36**, 99–134.

MORAN, S. C., NEWHALL, C. & ROMAN, D. C. 2011. Failed magmatic eruptions: Late-stage cessation of magma ascent. *Bulletin of Volcanology*, **73**, 115–122.

MULLER, O. H. & POLLARD, D. D. 1977. The stress state near Spanish Peaks, Colorado, determined from a dike pattern. *Pure and Applied Geophysics*, **115**, 69–86.

MURPHY, B. S., METCALFE, K. S. *ET AL.* 2012. Magma reservoir rupture beneath a Venusian edifice: When does lithospheric flexure become significant? *In*: *43rd*

Lunar and Planetary Science Conference, held 19–23 March 2012 at The Woodlands, Texas. Lunar and Planetary Institute, Houston, TX, Abstract 1060.

Newhall, C. G. & Dzurisin, D. 1988. *Historical Unrest at Large Calderas of the World, Volumes 1 & 2. United States Geological Survey Bulletin*, **1855**.

Newman, A., Dixon, T., Ofoegbu, G. & Dixon, J. 2001. Geodetic and seismic constraints on recent activity at Long Valley Caldera, California: evidence for viscoelastic rheology. *Journal of Volcanology and Geothermal Research*, **105**, 183–206.

Newman, A., Dixon, T. & Gourmelen, N. 2006. A four-dimensional viscoelastic deformation model for Long Valley Caldera, California, between 1995 and 2000. *Journal of Volcanology and Geothermal Research*, **150**, 244–269.

Nur, A. & Walder, J. 1990. Time-dependent hydraulics of the Earth's crust. *In*: *The Role of Fluids in Crustal Processes*. National Academy Press, Washington, DC, 113–127.

Owen, S., Segall, P., Freymueller, J., Mikijus, A., Denlinger, R., Arnadottir, T., Sako, M. & Burgmann, R. 1995. Rapid deformation of the south flank of Kilauea volcano, Hawaii. *Science*, **267**, 1328–1332.

Owen, S., Segall, P., Lisowski, M., Miklius, A., Murray, M., Bevis, M. & Foster, J. 2000. January 30, 1997 eruptive event on Kilauea volcano, Hawaii, as monitored by continuous GPS. *Geophysical Research Letters*, **27**, 2757–2760.

Parfitt, E. A. & Head, J. W. 1993. Buffered and unbuffered dike emplacement on Earth and Venus: implications for magma reservoir size, depth, and rate of magma replenishment. *Earth, Moon and Planets*, **61**, 249–281.

Parfitt, E. A., Wilson, L. & Head, J. W. 1993. Basaltic magma reservoirs: factors controlling their rupture characteristics and evolution. *Journal of Volcanology and Geothermal Research*, **55**, 1–14.

Parks, M. M., Biggs, J. *et al.* 2012. Evolution of Santorini volcano dominated by episodic and rapid fluxes of melt from depth. *Nature Geoscience*, **5**, 749–754.

Pinel, V. & Jaupart, C. 2000. The effect of edifice load on magma ascent beneath a volcano. *Philosophical Transactions of the Royal Society of London*, **358**, 1515–1532.

Pinel, V. & Jaupart, C. 2003. Magma chamber behavior beneath a volcanic edifice. *Journal of Geophysical Research*, **108**, 2072, http://dx.doi.org/10.1029/2002JB001751

Pinel, V. & Jaupart, C. 2004. Magma storage and horizontal dyke injection beneath a volcanic edifice. *Earth and Planetary Science Letters*, **221**, 245–262.

Pinel, V. & Jaupart, C. 2005. Caldera formation by magma withdrawal from a reservoir beneath a volcanic edifice. *Earth and Planetary Science Letters*, **230**, 273–287.

Poland, M. P., Moats, W. P. & Fink, J. H. 2008. A model for radial dike emplacement in composite cones based on observations from Summer Coon volcano, Colorado, USA. *Bulletin of Volcanology*, **70**, 861–875.

Pritchard, M. E. & Simons, M. 2004. An InSAR-based survey of volcanic deformation in the central Andes. *Geochemistry, Geophysics, Geosystems*, **5**, Q02002, http://dx.doi.org/10.1029/2003GC000610

Radebaugh, J., Keszthelyi, L. P., McEwen, A. S., Turtle, E. P., Jaeger, W. & Milazzo, M. 2001. Paterae on Io: a new type of volcanic caldera? *Journal of Geophysical Research*, **106**, 33,005–33,020.

Roche, O., Druitt, T. H. & Merle, O. 2000. Experimental study of caldera formation. *Journal of Geophysical Research*, **105**, 395–416.

Ronchin, E., Masterlark, T., Molist, J. M., Saunders, S. & Tao, W. 2013. Solid modeling techniques to build 3D finite element models of volcanic systems: an example from the Rabaul caldera system, Papua New Guinea. *Computers & Geosciences*, **52**, 325–333.

Russo, G., Giberti, G. & Sartoris, G. 1997. Numerical modeling of surface deformation and mechanical stability of Vesuvius volcano, Italy. *Journal of Geophysical Research*, **102**, 24,785–24,800.

Rymer, H. & Williams-Jones, G. 2000. Volcanic eruption prediction: magma chamber physics from gravity and deformation measurements. *Geophysical Research Letters*, **27**, 2389–2392.

Sanchez, L. & Shcherbakov, R. 2012. Scaling properties of planetary calderas and terrestrial volcanic eruptions. *Nonlinear Processes in Geophysics*, **19**, 585–593.

Sartoris, G., Pozzi, J. P., Phillipe, C. & Le Mouel, J. L. 1990. Mechanical stability of shallow magma chambers. *Journal of Geophysical Research*, **95**, 5141–5151.

Schöpa, A. & Annen, C. 2013. The effects of magma flux variations on the formation and lifetime of large silicic magma chambers. *Journal of Geophysical Research*, **118**, 926–942.

Schultz, R. A. 1995. Limits on strength and deformation properties of jointed basaltic rock masses. *Rock Mechanics and Rock Engineering*, **28**, 1–15.

Segall, P. 2013. Volcano deformation and eruption forecasting. *In*: Pyle, D. M., Mather, T. A. & Biggs, J. (eds) *Remote Sensing of Volcanoes and Volcanic Processes: Integrating Observation and Modelling*. Geological Society, London, Special Publications, **380**. First published online March 20, 2013, http://dx.doi.org/10.1144/SP380.4

Shuler, A., Ekstrom, G. & Nettles, M. 2013. Physical mechanisms for vertical-CLVD earthquakes at active volcanoes. *Journal of Geophysical Research*, **118**, 1569–1586, http://dx.doi.org/10.1002/jgrb.50131

Sigurdsson, H., Houghton, B., Rymer, H., Stix, J. & McNutt, S. (eds) 2000. *Encyclopedia of Volcanoes*. Academic Press, San Diego, CA.

Simpson, G. 2001. Influence of compression-induced fluid pressures on rock strength in the brittle crust. *Journal of Geophysical Research*, **106**, 19,465–19,478.

Simpson, R. W. 1997. Quantifying Anderson's fault types. *Journal of Geophysical Research*, **102**, 17,909–17,919.

Sparks, S. R. J., Sigurdsson, H. & Wilson, L. 1977. Magma mixing: a mechanism for triggering acid explosive eruptions. *Nature*, **267**, 315–318.

Sturkell, E., Sigmundsson, F., Geirsson, H., Ólafsson, H. & Theodórsson, T. 2008. Multiple volcano

deformation sources in a post-rifting period: 1989–2005 behavior of Krafla, Iceland constrained by leveling, tilt and GPS observations. *Journal of Volcanology and Geothermal Research*, **177**, 405–417.

Swarbrick, R. E. & Osborne, M. J. 1998. Mechanisms that generate abnormal pressures: an overview. *In*: Law, B. E., Ulmishek, G. F. & Slavin, V. I. (eds) *Abnormal Pressures in Hydrocarbon Environments*. American Association of Petroleum Geologists, Memoirs, **70**, 13–34.

Tait, S., Jaupart, C. & Vergniolle, S. 1989. Pressure, gas content and eruption periodicity of a shallow, crystallizing magma chamber. *Earth and Planetary Science Letters*, **92**, 107–123.

Timoshenko, S. & Goodier, J. N. 1951. *Theory of Elasticity*. McGraw-Hill, New York.

Trasatti, E., Giunchi, C. & Bonafede, M. 2003. Effects of topography and rheological layering on ground deformation in volcanic regions. *Journal of Volcanology and Geothermal Research*, **122**, 89–110.

Trasatti, E., Giunchi, C. & Bonafede, M. 2005. Structural and rheological constraints on source depth and overpressure estimates at the Campi Flegrei caldera, Italy. *Journal of Volcanology and Geothermal Research*, **144**, 105–118.

Trasatti, E., Giunchi, C. & Agostinetti, N. P. 2008. Numerical inversion of deformation caused by pressure sources: application to Mount Etna (Italy). *Geophysical Journal International*, **172**, 873–884.

Watts, A. B. 2001. *Isostacy and Flexure of the Lithosphere*. Cambridge University Press, Cambridge.

Wilson, L. & Head, J. W. 1994. Mars: review and analysis of volcanic eruption theory and relationships to observed landforms. *Reviews of Geophysics*, **32**, 221–263.

Xu, S.-S., Nieto-Samaniego, A. F. & Alaniz-Alvarez, S. A. 2013. Emplacement of pyroclastic dykes in Riedel shear fraxtures: an example from Sierra de San Miguelito, central Mexico. *Journal of Volcanology and Geothermal Research*, **250**, 1–8.

Yang, X., Davis, P. & Dietrich, J. 1988. Deformation from inflation of a dipping finite prolate spheroid in an elastic half-space as a model for volcanic stressing. *Journal of Geophysical Research*, **93**, 4249–4257.

Zimbelman, J. R. & Gregg, T. K. P. (eds) 2000. *Environmental Effects on Volcanic Eruptions*. Kluwer Academic, New York.

Zoback, M. D. 2010. *Reservoir Geomechanics*. Cambridge University Press, New York.

Zuber, M. T. & Mouginis-Mark, P. J. 1992. Caldera subsidence and magma chamber depth of the Olympus Mons volcano, Mars. *Journal of Geophysical Research*, **97**, 18,295–18,307.